communications biology

Article

https://doi.org/10.1038/s42003-024-06605-8

Human T-cell receptor triggering requires inactivation of Lim kinase-1 by Slingshot-1 phosphatase

Check for updates

Álvaro Gómez-Morón[1,2,3,11], Sergio Alegre-Gómez[1,2,11], Rocio Ramirez-Muñoz[1,2], Alicia Hernaiz-Esteban[1,2], Carlos Carrasco-Padilla[1,2], Camila Scagnetti[3,4], Óscar Aguilar-Sopeña[1,2], Marta García-Gil[1,2], Aldo Borroto[5], Raul Torres-Ruiz[6,7,8], Sandra Rodriguez-Perales[6], Francisco Sánchez-Madrid[3,9,10], Noa Beatriz Martín-Cófreces[3,4,9,10,12] ✉ & Pedro Roda-Navarro[1,2,12] ✉

Actin dynamics control early T-cell receptor (TCR) signalling during T-cell activation. However, the precise regulation of initial actin rearrangements is not completely understood. Here, we have investigated the regulatory role of the phosphatase Slingshot-1 (SSH1) in this process. Our data show that SSH1 rapidly polarises to nascent cognate synaptic contacts and later relocalises to peripheral F-actin networks organised at the mature immunological synapse. Knockdown of SSH1 expression by CRISPR/Cas9-mediated genome editing or small interfering RNA reveal a regulatory role for SSH1 in CD3ε conformational change, allowing Nck binding and proper downstream signalling and immunological synapse organisation. TCR triggering induces SSH1-mediated activation of actin dynamics through a mechanism mediated by Limk-1 inactivation. These data suggest that during early TCR activation, SSH1 is required for rapid F-actin rearrangements that mediate initial conformational changes of the TCR, integrin organisation and proximal signalling events for proper synapse organisation. Therefore, the SSH1 and Limk-1 axis is a key regulatory element for full T cell activation.

T cells scan antigen-presenting cells (APCs) through exploratory contacts dependent on microvilli enriched in filamentous actin (F-actin), which can be stabilised when the T-cell receptor (TCR) encounters a cognate peptide bound to the major histocompatibility complex (pMHC)[1]. Activation of the TCR triggers the rearrangement of the tubulin and actin cytoskeleton during the immunological synapse (IS), which in turn are required for sustained T cell activation and effector function[2,3]. In this regard, actin polymerisation at TCR clustering sites is needed for TCR triggering and nascent signalling[4,5] and promotes the association of Nck (non-catalytic region of tyrosine kinase) with the CD3ε invariant chain of the TCR to enable downstream signalling[6,7].

The actin severing and depolymerising factor cofilin promotes actin polymerisation by increasing the local concentration of actin barbed ends and the pool of available globular actin in vitro[8]. In T cells, cofilin participates in cytoskeletal rearrangements downstream of co-stimulatory signals[3,9,10], is recruited to the contact area between T cells and APCs and is critical for LFA-1 clustering[11]. Cofilin also regulates NF-κB translocation to the nucleus for cytokine production[12,13]. Consistent with an important role during T cell activation, active species of cofilin increase in in vitro expanded, antigen-experienced T cells[14]. Cofilin has been proposed to mediate the differentiation of αβ but not γδ T cells[15], but the

[1]Department of Immunology, Ophthalmology and ENT, School of Medicine, Universidad Complutense de Madrid, Madrid, Spain. [2]12 de Octubre Health Research Institute (imas12), 28040 Madrid, Spain. [3]Immunology Service, Instituto de Investigación Sanitaria del Hospital Universitario La Princesa, IIS-Princesa, UAM, 28006 Madrid, Spain. [4]Videomicroscopy Unit, Instituto de Investigación Sanitaria del Hospital Universitario La Princesa, IIS-Princesa, UAM, 28006 Madrid, Spain. [5]Centro de Biología Molecular Severo Ochoa, Campus de Cantoblanco, 28049 Madrid, Spain. [6]Molecular Cytogenetics and Genome Editing Unit, Human Cancer Genetics Program, Centro Nacional de Investigaciones Oncológicas (CNIO), 28029 Madrid, Spain. [7]Division of Hematopoietic Innovative Therapies, Biomedical Innovation Unit, Centro de Investigaciones Energéticas, Medioambientales y Tecnologicas (CIEMAT); Advanced Therapies Unit, Instituto de Investigacion Sanitaria Fundacion Jiménez Díaz; Centro de Investigación Biomédica en Red de Enfermedades Raras (CIBERER), 28040 Madrid, Spain. [8]Advanced Therapies Unit, Instituto de Investigación Sanitaria Fundación Jiménez Díaz (IIS-FJD, UAM), 28040 Madrid, Spain. [9]Area of Vascular Pathophysiology, Laboratory of Intercellular Communication, Fundación Centro Nacional de Investigaciones Cardiovasculares-Carlos III, 28029 Madrid, Spain. [10]CIBER de Enfermedades Cardiovasculares (CIBERCV), Madrid, Spain. [11]These authors contributed equally: Álvaro Gómez-Morón, Sergio Alegre-Gómez. [12]These authors jointly supervised this work: Noa Beatriz Martín-Cófreces, Pedro Roda-Navarro. ✉e-mail: noa.martin@salud.madrid.org; proda@ucm.es

underlying mechanisms explaining the role of cofilin in T cells remain unknown.

Cofilin activity is regulated by the phosphorylation/dephosphorylation balance of the serine 3 (Ser3) residue. Several phosphatases have been described as activators of cofilin, such as the Ser-Thr phosphatases PP1 and PP2A[16], chronophin, and the family of dual-specific phosphatases Slingshot (SSHs; SSH1, SSH2 and SSH3); conversely, inactivation of cofilin is achieved by phosphorylation by Lim and testicular protein kinases (LIMK and TESK, respectively)[17]. SSH1 and SSH2 have higher phosphatase activity against cofilin than SSH3 and have bundling activity on actin filaments, which greatly enhances their phosphatase activity against cofilin[18]. These proteins can also dephosphorylate Limk-1, leading to its inactive state. Thus, the phosphatase activity of the SSHs is expected to promote ultrasensitive activation of cofilin, which has been proposed to promote efficient T cell responses[14].

The role of SSHs during TCR stimulation has not been characterised and this issue was investigated here. Endogenous SSH1 expression correlates with cofilin activation in activated T cells, suggesting a regulatory role for SSH1 during this process. SSH1 is rapidly recruited to nascent cognate interactions with APCs, where it activates cofilin and regulates the TCR conformational change that exposes the proline-rich sequence of the CD3ε invariant chain for Nck recruitment. Consistent with these observations, SSH1-deficient cells show defective T cell activation and impaired synaptic organisation of the TCR and integrins, as well as reduced cytokine production.

Results

SSH1 is upregulated by T-cell activation and recruited to the IS

To investigate the potential role of SSH1 during human CD4 T-cell activation and differentiation, SSH1 expression was assessed. Western blot analysis revealed an induction of the expression of the phosphatase during activation of primary human CD4 T cells isolated from PBMCs, after 16–40 h of TCR stimulation and co-stimulation engagement in the presence of IL-12 (Fig. 1a). The higher expression levels were reached and maintained for approximately 88 h during CD4 T cell expansion and differentiation (Fig. 1a, b and Supplementary Fig. 1a, b). This increased expression correlated with the concomitant activation of cofilin, as shown by the decrease in the phosphorylation level of Ser3 (Fig. 1a, b). These results indicate that increased SSH1 expression supports cofilin activation in stimulated CD4 T cells. Resting CD4 T cells expressed almost undetectable levels of SSH1 compared to their counterpart blasted CD4 T cells (Fig. 1a and Supplementary Fig. 1a, b). Since cofilin is a known regulator of actin dynamics, which is essential for T cell activation, these data suggest that SSH1 may be a regulator of F-actin networks in T cells and that it may play a relevant role during cognate synaptic contacts with APCs.

Endogenous localisation of SSH1 was studied by immunofluorescence of synaptic contacts established by in vitro SEE-stimulated, primary human CD4 T cells isolated from PBMCs to generate expanded lymphoblasts. SEE-preloaded Raji B cells were used as APCs. Unstimulated lymphoblasts in contact with Raji B cells did not induce the localisation of SSH1 at the synaptic contacts. The presence of SEE induced a rapid polarisation of SSH1 to the IS, accompanied by the expected accumulation of CD3ε and increased local F-actin polymerisation (Fig. 1c, d). SSH1 localised mainly to F-actin networks at the periphery of the mature IS, an area from which CD3ε was excluded (Fig. 1e). Consistent with this, a clear co-localisation of SSH1 and F-actin was found (Fig. 1e, f).

Dynamic recruitment of SSH1 to the immunological synapse depends on F-actin networks

The dynamic polarisation of SSH1 and CD3ζ to the synapse was tracked by live-cell confocal microscopy in CH7C17 Jurkat T cells overexpressing GFP-SSH1 and CD3ζ-mCherry fluorescent fusion proteins. HOM2 lymphoblastoid B cells were used as APCs to present the influenza haemagglutinin peptide (HAp) specifically recognised by the TCR expressed by CH7C17. GFP-SSH1 polarisation at the IS was observed as soon as the T cell initiated early exploratory contacts with HAp-loaded HOM2 cells. As a result, there was a rapid and clear accumulation of the protein at the contact sites, observed as early as 30 s. After 130 s of interaction, GFP-SSH1 and CD3ζ-mCherry were located in peripheral and central areas of the IS, respectively (Fig. 2a, b and Supplementary Movie 1). These data showed an early delivery of SSH1 to nascent cognate interactions and its distribution to the peripheral sites of the mature synapse.

To ascertain whether GFP-SSH1 localisation at the synapse depends on F-actin integrity, E6-1 Jurkat T cells overexpressing GFP-SSH1 were allowed to form synapses with SEE-preloaded Raji B cells and treated with latrunculin-A (Lat-A), which prevents F-actin polymerisation. Lat-A was added after 5 min of T-B cognate interaction to disrupt local F-actin at the synapse. Lat-A blocked the accumulation of GFP-SSH1 and F-actin, but not CD3ε, at the IS (Fig. 2c, d). Pearson´s coefficient showed that Lat-A treatment reduced the co-localisation at the synapse of GFP-SSH1 with F-actin but not with CD3ε (Fig. 2c–e). To further prove the role of the actin cytoskeleton in SSH1 dynamics, cytochalasin D (Cyto-D), which promotes F-actin depolymerisation[18], was used in a similar set of experiments, paralleling the effect of Lat-A on SSH1 localisation. However, Cyto-D disruption of F-actin also cleared CD3ε from the already formed synapse, preventing polarisation (Supplementary Fig. 2a, b). Changes in the Pearson's coefficient were similar upon treatment with Cyto-D and Lat-A; SSH1 and F-actin colocalisation decreased, but that of SSH1 and CD3ε remained unchanged (Supplementary Fig. 2a, c). This indicates that the location of SSH1 at the IS is highly dynamic and depends on the balance between actin depolymerisation and polymerisation, whereas CD3ε, after an initial relocalisation, can be detected at the synaptic contact in the absence of new actin polymerisation, probably due to TCR-MHC binding[19]. These data raise the hypothesis that SSH1 localisation may depend on the organisation of F-actin networks established at the synapse during cognate interactions between T and B cells.

SSH1 regulates TCR signalling and T-cell activation

To investigate the relevance of SSH1 in TCR activation, early signalling activated downstream of the TCR was assessed in CRISPR/Cas9-mediated genome-edited E6-1 Jurkat T cells to knockout SSH1 expression (*SSH1* KO cells) (Supplementary Fig. 3a). The initial polyclonal population of edited cells already showed reduced levels of SSH1 compared to control cells and no changes in cofilin activation were observed in these quiescent cells (Supplementary Fig. 3b). To isolate knockout cells, clones were generated by limiting dilution (Supplementary Fig. 3c) and the DNA sequencing of one of the clones (clone 12), confirmed the specific editing of the gene, in which an insertion of three base pairs generates a premature stop codon in the region upstream of the B (binding) and the P (phosphatase) domains (Supplementary Fig. 3d). The phosphorylation state of cofilin in the clone 12 or in the pool of four knockout clones (purple squares in Supplementary Fig. 3c) was not different from that in control cells (Supplementary Fig. 3d). These data indicate that the phosphorylation status of cofilin in resting Jurkat cells is not regulated by SSH1.

The pool of *SSH1* KO clones, which potentially avoids problems of clonal selection, was tested for expression of cell surface markers by using specific antibodies and flow cytometry. Similar expression of activation and adhesion receptors, CD3, CD4 and integrins such as LFA-1 and VLA-4 was observed compared to control cells (Supplementary Fig. 4). These cells were activated or not with SEE-preloaded Raji B cells for the indicated times, and signalling pathways emanating from the TCR were studied. The level of phosphorylation of molecules involved in the early signalling pathways was reduced by the absence of SSH1 (Fig. 3a, c). Different antibodies were used against specific residues known to be relevant, such as pY83 in the first ITAM (immunoreceptor tyrosine-based activation motif) of CD3ζ and pY493 of ZAP70, two molecules that form part of the early signalling module of the TCR[20,21] and showed decreased activation ratios (Fig. 3a). The signalosome of LAT, a scaffolding protein downstream of the TCR, was also analysed by probing pY132 LAT, pY783 PLCγ1 and pY145 SLP76[22] (Fig. 3b); pY132 LAT decreased at early times (2 and 5 min) and

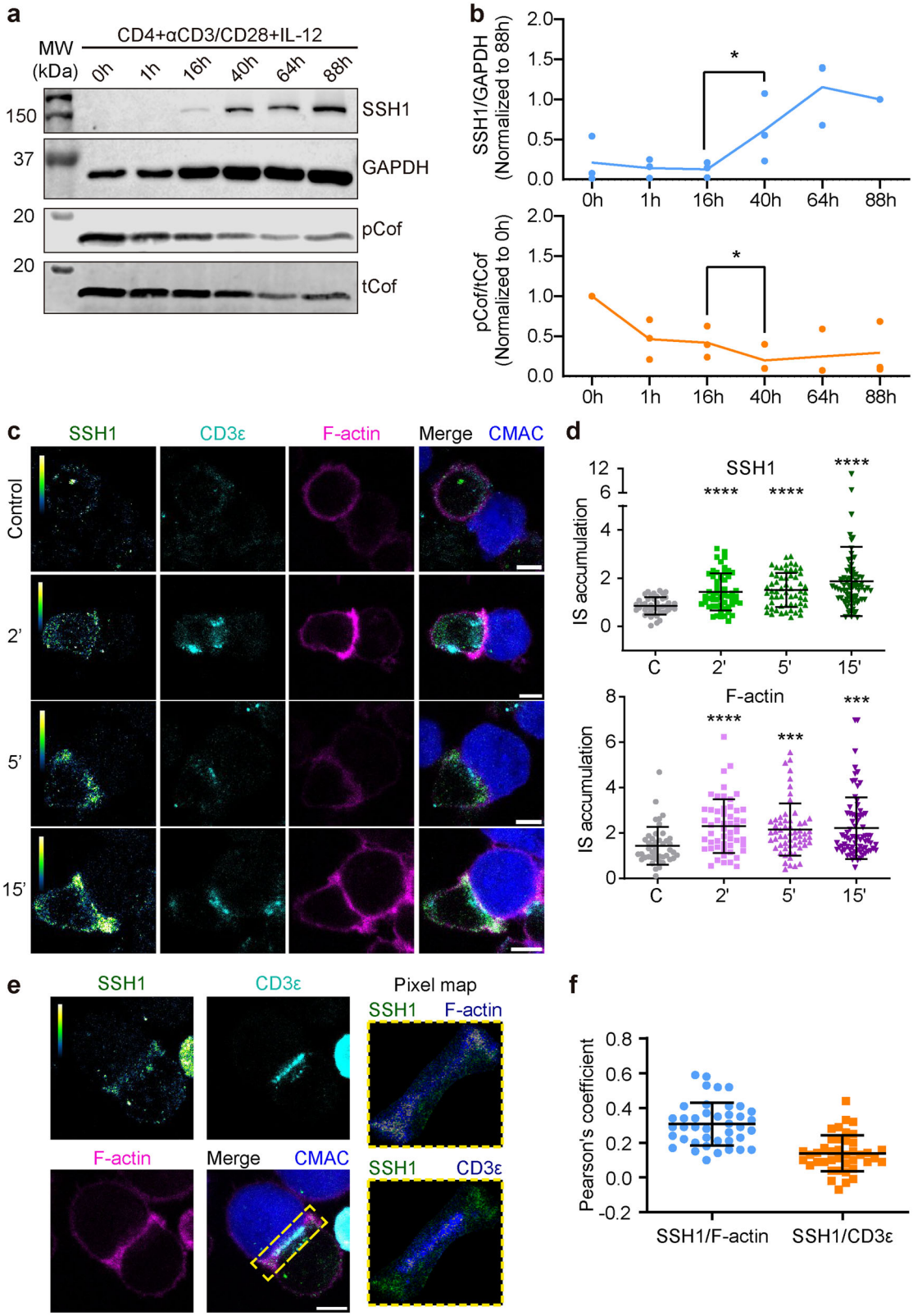

Fig. 1 | SSH1 expression and distribution in activated CD4 T cells. a Western blot showing the expression of SSH1, GAPDH, phosphorylated cofilin at Ser3 (pCof) and total cofilin (tCof) in peripheral blood CD4 T cells stimulated for the indicated times in hours (h). **b** Graphs, ratios of SSH1 vs. GAPDH and pCof vs. tCof. Densitometric values were normalised to 88 and 0 h, respectively. Individual experiments are shown by dots and lines represent the mean value ($n = 3$), two-tailed paired t-test. **c** Fluorescence images of SEE-expanded human primary CD4 T lymphoblasts conjugated with CMAC-labelled, SEE-loaded or unloaded Raji B cells. SSH1, pseudocolour or green in the merged image; CD3ε (cyan) and F-actin (magenta). Bar, 5 µm. **d** Graphs, SSH1 and F-actin polarisation at the IS. Graph, mean ± SD; control, $n = 44$; SEE, $n = 60$ cells analysed from three independent experiments; two-tailed unpaired t-test. **e** Long-term synapse from (**c**). Yellow rectangles, magnifications showing co-localisation pixel map (white pixels) of SSH1 (green) with F-actin (blue; top) or CD3ε (blue; bottom). **f** Graphs, Pearson's correlation coefficient obtained in individual cell conjugates analysed (blue and orange symbols). Lines indicate the mean ± SD; (SSH1/F-actin and SSH1/CD3, $n = 41$ cells analysed from three independent experiments). Two-tailed paired t-test. $^{*}p < 0.05$, $^{***}p < 0.001$, $^{****}p < 0.0001$. See also Supplementary Fig. 1.

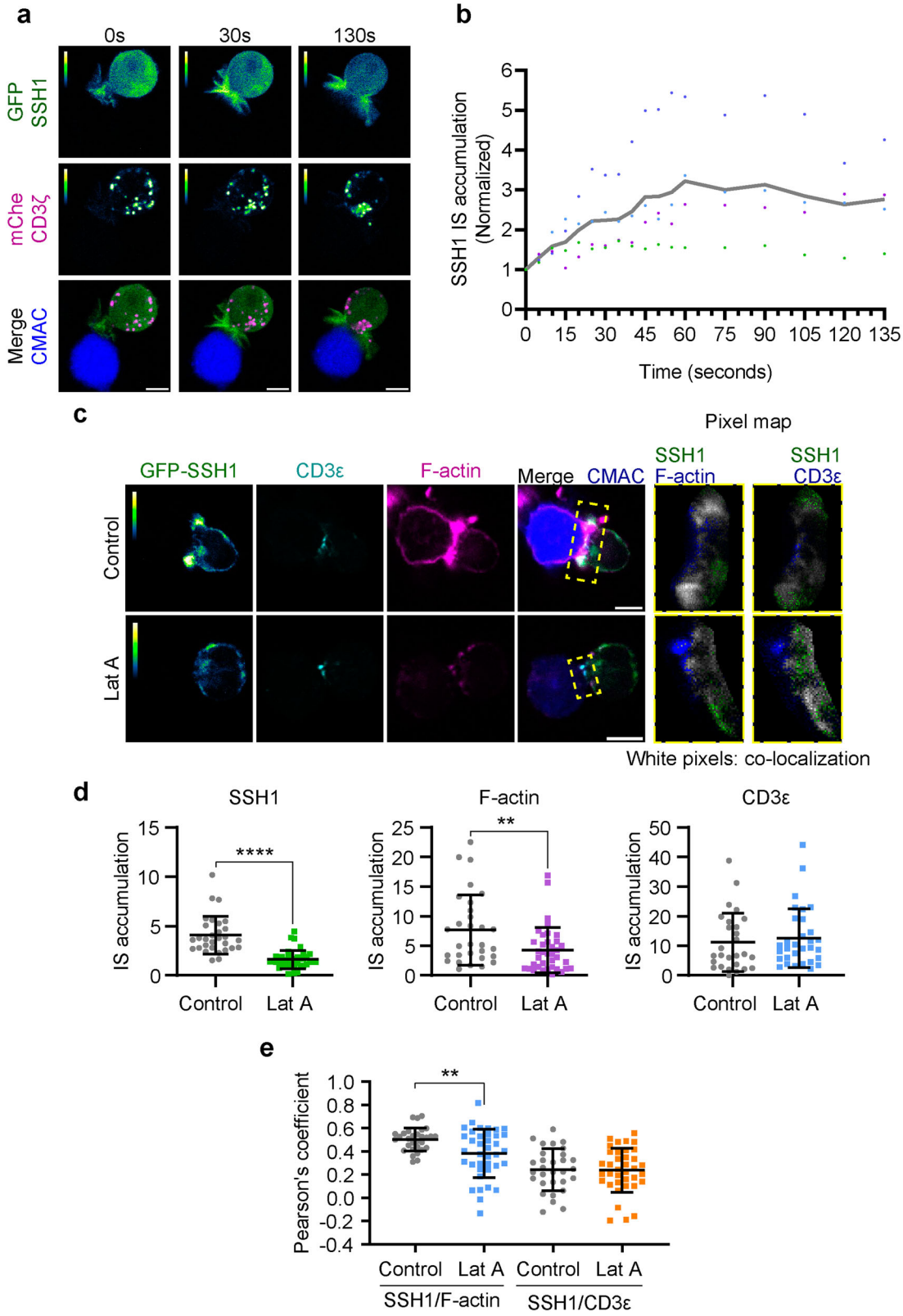

PLCγ1 showed a decreased activation ratio at all times examined. The extent of SLP76 phosphorylation showed similar levels than control cells at 5 and 15 min, with decreased activation at early times (Fig. 3b). Finally, ERK1/2 showed decreased activation at all the times tested, with the greatest differences observed at shorter times of activation (Fig. 3c). Similar decrease in TCR downstream signalling was observed in SSH1 silenced CH7C17 Jurkat T cells stimulated with HAp-loaded HOM2 cells (Supplementary Fig. 5a). The phosphorylation of Y83 CD3ζ, Y783 PLCγ1, Y493 ZAP70 and T202/Y204 ERK1/2 were decreased in cells with reduced SSH1 expression (Supplementary Fig. 5b–d). To address whether this defect in proximal signalling is relevant to T cell activation, CD69 expression was analysed by flow cytometry in experiments with control and *SSH1* KO JK

Fig. 2 | Dynamic accumulation of overexpressed SSH1 at the IS is dependent on F-actin integrity. a Confocal fluorescence images from a time-lapse assay showing the polarisation of GFP-SSH1 (pseudocolour or green in the merged images) and mCherry-CD3ζ (pseudocolour or magenta in the merged images) to the IS in conjugates of transfected CH7C17 Jurkat T cells and CMAC-labelled, HAp-preloaded HOM2 cells. Bar, 5 µm. **b** Graph, accumulation of SSH1 at the IS after initial contact between cells (0 s), normalised to 0 s; ($n = 4$) individual cells are shown by coloured dots and the grey line represents the mean value. **c** Confocal fluorescence images showing cell conjugates of GFP-SSH1-overexpressing E6-1 Jurkat T cells and CMAC-labelled, SEE-preloaded Raji cells, treated or not with Latrunculin A (Lat-A); GFP-SSH1, pseudocolour or green in the merged picture; CD3ε, cyan; F-actin, magenta. Bar, 5 µm. Yellow squares, magnified long-term synapses; white pixels indicate co-localisation of SSH1 (green) and F-actin (blue; left) or CD3ε (blue; right). **d** Graphs showing SSH1, F-actin and CD3ε accumulation at the IS. Symbols are cell conjugates measured. **e** Pearson's correlation coefficient for co-localisation between SSH1/F-actin and SSH1/CD3ε. Symbols are conjugates measured. Data are mean ± SD; control, $n = 30$; Lat-A, $n = 37$ cells analysed from three independent experiments; two-tailed unpaired *t*-tests. $^{**}p < 0.01$; $^{****}p < 0.0001$. See also Supplementary Fig. 2.

T cells stimulated by SEE-preloaded Raji B cells. *SSH1* KO cells showed reduced CD69 expression (Fig. 3d and gating strategy in Supplementary Fig. 6) and reduced IL-2 secretion as measured by ELISA (Fig. 3e). These results suggest that SSH1 is required for full T cell activation and that its action is exerted very early after TCR activation, affecting several signalling pathways.

SSH1 is required for TCR conformational change

To determine whether SSH1 directly regulates the TCR, control and *SSH1* KO cells were stimulated with anti-CD3 plus anti-CD28 monoclonal antibodies for the indicated times and subjected to GST-Nck pulldown. Nck binds to the TCR by interacting with the CD3ε invariant chain when it changes its conformation due to the engagement of a specific antigen[6]. We observed that the interaction of GST-Nck with the TCR (assessed by CD3ζ pull-down) was reduced in *SSH1* KO cells at early time points, either the 15 kDa form or the phosphorylated 21 kDa form[23,24] (Fig. 4a), suggesting that the TCR requires SSH1 to enable efficient CD3ε conformational change leading to activation of the downstream signalling pathways. Cells from these assays were probed for activation with pT202/Y204 ERK1/2 and pY83 CD3ζ (Supplementary Fig. 7), reinforcing the idea of a defect in the early phosphorylation of CD3ζ observed previously (Fig. 3a). To determine whether the absence of SSH1 prevents the open conformation of the CD3ε dimer, we used APA1/1, a specific monoclonal antibody that recognises a conformational epitope on the intracellular part of the dimer of CD3ε chains when active[6,25]. Polyclonal activation of T cells with stimulating monoclonal antibodies and detection by flow cytometry indicated that *SSH1* KO cells showed reduced activation in terms of active TCR (Fig. 4b). Indeed, reduced active CD3ε was observed at the contacts of *SSH1* KO cells with APCs, with decreased APA1/1 labelling in central areas of IS established by *SSH1* KO cells. The localisation of active CD3ε was close to peripheral F-actin, as shown in the 3D reconstruction of the T-APC contact area (Fig. 4c; 3D merge). A reduced accumulation of total CD3ε was also observed by extracellular epitope staining, with a similar distribution (Fig. 4d; 3D merge). These results suggest that SSH1 is an early regulator of the active conformation of the TCR/CD3 complex upon contact with cognate antigens, and that this may influence TCR recruitment to the synapse, which is required for full T cell activation.

SSH1 links TCR-dependent actin-related pathways

The correlation between the increase in SSH1 expression and cofilin activation suggested that this phosphatase dephosphorylates and activates cofilin in lymphoblasts (Fig. 1a). To investigate this regulation of cofilin activity during T cell activation, control and *SSH1* KO cells were stimulated with SEE-preloaded Raji B cells. *SSH1* KO cells showed no expression of the protein (Fig. 5a). Phosphorylation of cofilin and Limk-1 was analysed in these cells by Western blot. The phosphorylation of Limk-1 was strongly increased in *SSH1* KO cells upon TCR activation with SEE-preloaded Raji B cells for the indicated times (Fig. 5b). The activation of Limk-1 correlated with a decrease in the activation of cofilin, as shown by the increased phosphorylation at Ser3 (Fig. 5b, c). To further characterise the cofilin regulatory module, phosphorylation of p21-activated kinase (PAK1), a protein involved in cofilin inhibition through phosphorylation and activation of Limk-1[26], was also determined. Consistent with what was observed for cofilin and Limk-1, *SSH1* KO cells showed increased phosphorylation of T402 PAK1 compared to control cells (Fig. 5d). To verify this regulatory role of PAK1 on the cofilin module via Limk-1, control and *SSH1* KO cells were treated with stimulatory anti-CD3 plus anti-CD28 antibodies for the indicated times and subjected to pulldown with GST-PAK-CRIB, which recognises active Rac1, a small GTPase involved in PAK1 activation and increase in actin dynamics[27]. Rac1 activation was increased in *SSH1* KO cells compared to control cells (Fig. 5e), suggesting that SSH1 is a negative regulator of Rac1 and PAK1, thereby controlling the level of activation of these proteins. These data suggest a role for SSH1 in activating cofilin during T cell stimulation by dephosphorylating Limk-1 and/or directly dephosphorylating cofilin, as well as controlling Rac1 activation. Altogether, these results support a role for SSH1 in regulating actin dynamics during TCR activation and synapse organisation.

SSH1-regulated actin dynamics enables integrin organisation

Consistent with our previous observations, microscopy experiments revealed that *SSH1* KO cells exhibited enhanced actin polymerisation at the IS established with SEE-loaded Raji B cells (Fig. 6a). Given the importance of actin dynamics in establishing cell asymmetry and centrosome polarisation upon TCR activation, we also analysed centrosome localisation in these cells and found a defect in centrosome translocation towards the IS in *SSH1* KO cells (Fig. 6a). To further evaluate the role of SSH1 in F-actin dynamics, control or *SSH1* KO cells expressing mCherry-β-actin were seeded over stimulatory surfaces coated with anti-CD3 monoclonal antibody and recombinant ICAM-1. Live cells were imaged by total internal reflection fluorescence microscopy (TIRFm) to follow the dynamics of the actin cytoskeleton polarised to the stimulatory surface. Kymographs were generated from the videos, and the displacement of the actin signal was analysed to measure the distance travelled over time (Fig. 6b, c and Supplementary Movie 2). *SSH1* KO cells showed increased actin retrograde flow at the lamellipodia, as shown by calculating the speed of particle displacement (Fig. 6d). The observed increase in F-actin polymerisation in *SSH1* KO cells was also detected by flow cytometry in time-course experiments upon activation with anti-CD3ε and CD28 stimulatory antibodies (Fig. 6e).

F-actin organisation is required to enable integrin organisation at the IS[28–31]. The integrin adhesion ring is established at the lamella/pSMAC thanks to mechanotransduction forces generated by contractile actomyosin arcs at this area of the IS and actin retrograde flow at the lamellipodium/dSMAC[32,33]. Confocal sections and 3D reconstructions showed that SSH1 is required for proper polarisation and positioning of the integrins LFA-1 and VLA-4 at T-B IS (Fig. 6f, g). This perturbed distribution of integrins is indicative of defective F-actin dynamics, as observed (Fig. 6a–e). These data support a role for SSH1 in regulating cofilin activity and promoting the required F-actin dynamics to achieve the canonical integrin distribution at mature IS.

SSH1 regulates Limk-1 in primary human CD4 T cells

To confirm the role of SSH1 in primary T cells, CD4 T cells isolated from healthy donors were silenced by nucleofecting small interfering RNAs (siRNAs) specific for the *SSH1* gene (siSSH1) or unspecific as control (siCtrl) (Supplementary Fig. 8a). Forty-eight hours post-transfection, CD4 T cells were assayed for their ability to regulate Limk-1 and cofilin activity through phosphorylation upon TCR and CD28 stimulation (Fig. 7a, b). Limk-1 phosphorylation in siCtrl transfected cells decreased rapidly after

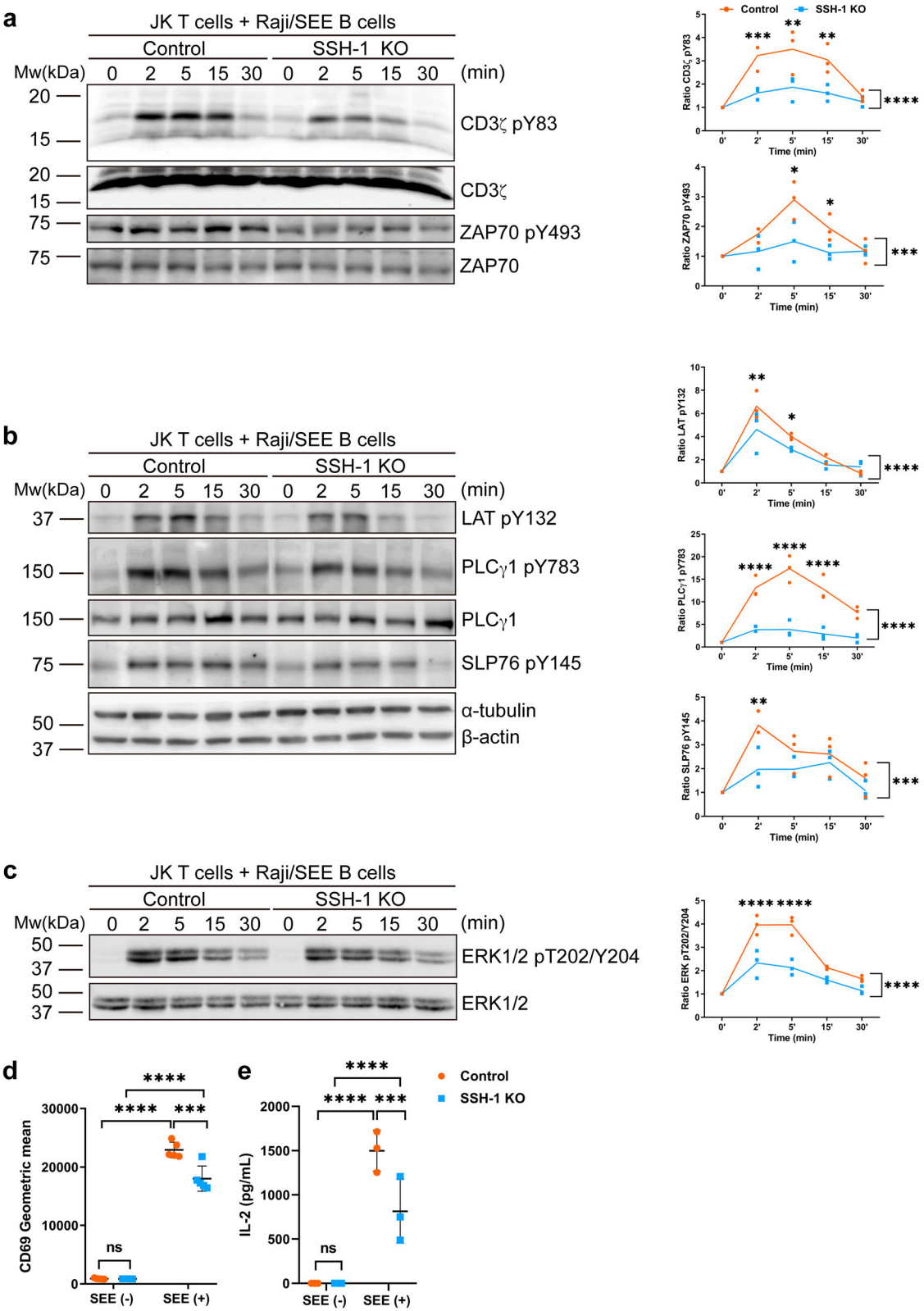

Fig. 3 | SSH1 regulates TCR signalling and T cell activation in Jurkat T cells. Western blots showing the phosphorylation kinetics of (**a**) pY83 CD3ζ and pY493 ZAP70, (**b**) pY132 LAT, pY783 PLCγ1 and pY145 SLP76, and (**c**) pT202/Y204 ERK 1/2 in control and *SSH1* KO JK T cells conjugated with SEE-preloaded or not Raji B cells for the indicated times. Graphs, ratio of phosphorylation to total protein normalised to unstimulated control. **d** Graph showing the average geometric mean of CD69 in control and *SSH1* KO JK T cells conjugated with SEE-preloaded or not Raji B cells for 18 h. **e** Secretion of IL-2 by control and *SSH1* KO cells conjugated with SEE-preloaded Raji cells for 18 h. Data are individual experiments shown as dots and lines representing the mean value (**a**–**c**) or mean ± SD (**d**, **e**); **a**–**c** $n = 3$; **d** $n = 5$; **e** $n = 3$, two-way ANOVA. *$p < 0.05$; **$p < 0.01$; ***$p < 0.001$; ****$p < 0.0001$. See also Supplementary Figs. 3–6.

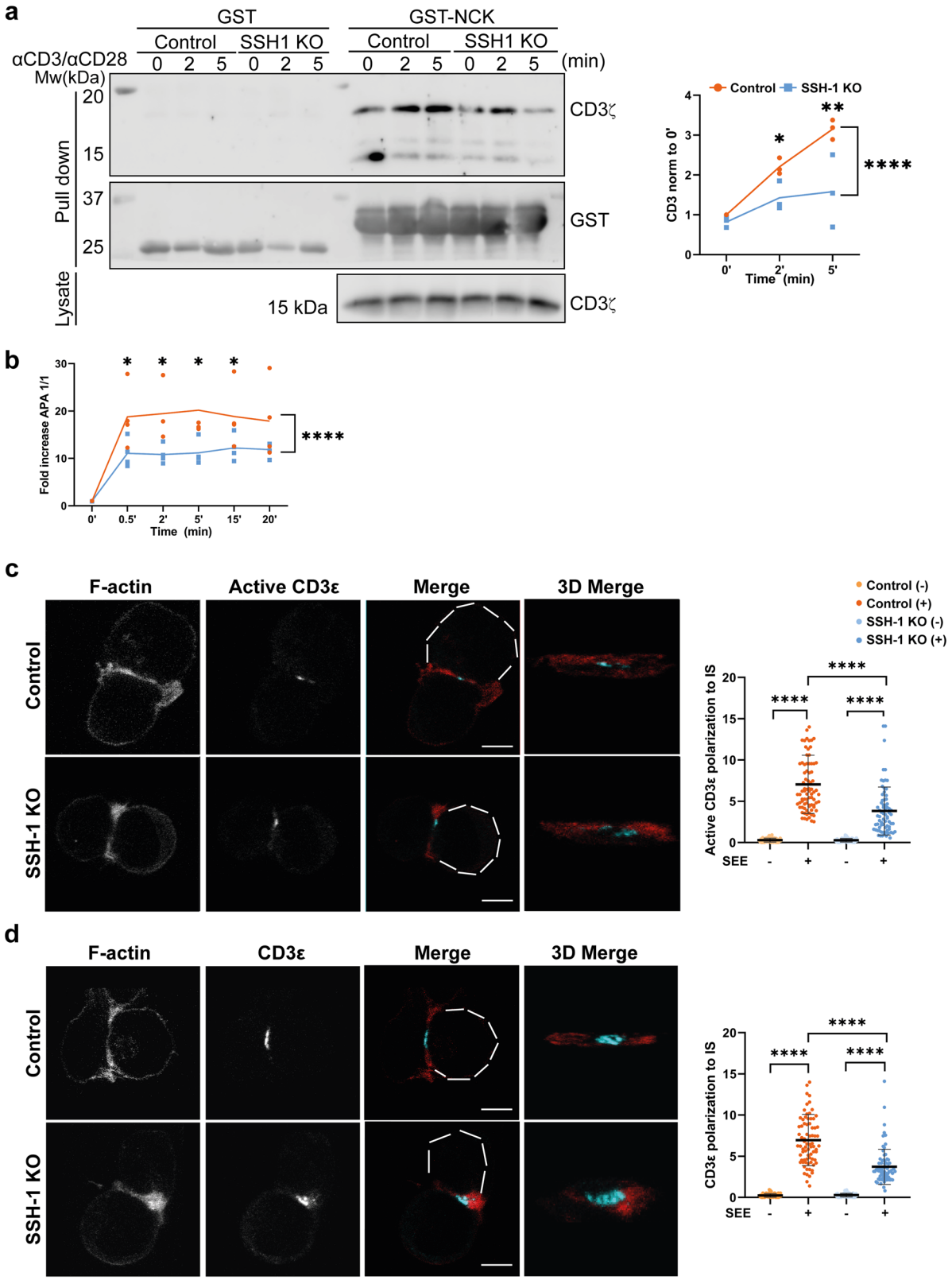

activation (2–5 min) and a recovery of phosphorylation was observed from 5 to 15 min. In contrast, in siSSH1 transfected cells, Limk-1 phosphorylation increased with activation and peaked at 5 min (Fig. 7a). Consequently, cofilin phosphorylation decreased with stimulation in siCtrl transfected cells, in contrast to siSSH1 transfected cells, which showed a constant increase in phosphorylation and thus a lack of activation of the protein upon TCR and CD28 stimulation (Fig. 7b). These data support the specific role of SSH1 as a phosphatase that regulates cofilin activity through Limk-1 in primary CD4 T cells after TCR and CD28 stimulation. Therefore, SSH1 regulates both the status of cofilin and Limk-1 phosphorylation in T cells, and the absence of SSH1 promotes impaired inactivation of Limk-1 and activation of cofilin, which would be expected to result in deregulated cytoskeletal rearrangement. These results demonstrate that SSH1 regulates F-actin dynamics during the IS assembly.

Fig. 4 | SSH1 is required for the TCR conformational change. a Western blot of pull-down assay with GST-Nck fusion protein as a bait for control or *SSH1* KO JK T cells. Activation was performed with soluble anti-CD3 and anti-CD28 antibodies for the indicated times. CD3ζ and GST are shown. CD3ζ levels in whole cell lysates are shown in the bottom row. Graph, quantification of CD3ζ bands normalised to the unstimulated control. **b** Graph, fold increase of the averaged geometric mean normalised to the unstimulated control of active CD3ε (detected by staining with the APA1/1 antibody) in control or *SSH1* KO JK T cells after activation with anti-CD3 and anti-CD28 antibodies for the indicated times. Fluorescence confocal images of control or *SSH1* KO JK T cells conjugated with SEE-preloaded Raji cells showing (**c**) active CD3ε (cyan) and F-actin (red) and (**d**) CD3ε (cyan) and F-actin (red). Bar, 5 μm. Graphs, polarisation ratio of (**c**) active CD3ε and (**d**) CD3ε at the IS. Symbols are cell conjugates measured. Data are individual experiments shown as dots and lines representing the mean value (**a**, **b**) or mean ± SD (**c**, **d**); **a** $n = 4$, two-way ANOVA; **b** $n = 4$, two-way ANOVA; **c** Ctrl(−) $n = 83$, Ctrl(+) $n = 80$, *SSH1* KO(−) $n = 75$, *SSH1* KO(+) $n = 73$, three independent experiments. Mann–Whitney test; **d** Ctrl(−) $n = 79$, Ctrl(+) $n = 77$, *SSH1* KO(−) $n = 70$, *SSH1* KO(+) $n = 76$, three independent experiments. Mann–Whitney test. $^{*}p < 0.05$; $^{**}p < 0.01$; $^{***}p < 0.001$. See also Supplementary Fig. 7.

SSH1 regulates CD4 T-cell activation

To determine whether this dysregulation of cofilin activity had an impact on early TCR signalling, pY83 CD3ζ and pY783 PLCγ1 were examined and found to have a similar decrease in their activity as in *SSH1* KO Jurkat cells (Fig. 7c). Defective TCR signalling in siSSH1 transfected cells corresponded to larger and irregular F-actin containing lamellae observed in confocal planes of synaptic-like contacts established across stimulating anti-CD3 plus anti-CD28 monoclonal antibody coated surfaces (Fig. 7d). 3D plots and quantification of MFI per area showed increased polymerisation of F-actin at the synapse-like contacts in siSSH1 cells (Fig. 7e, f). The organisation of CD3ζ relative to F-actin was also defective in SSH1 silenced CD4 T cells, with CD3ζ localisation being more external than in siCtrl CD4 T cells (Fig. 7g), resulting in enhanced co-localisation with F-actin (Fig. 7h). This distribution was also observed in siSSH1 CD4 T cells forming synapse-like structures with stimulating beads coated with anti-CD3 and anti-CD28 monoclonal antibodies to achieve a more canonical geometry of the IS (Fig. 7i). F-actin was increased in synapses formed by SSH1 silenced CD4 T cells and CD3ζ polarisation at the IS was reduced (Fig. 7i). These defects in T cell activation showed long-term consequences, as a reduction in CD69 and CD25 expression was observed in silenced SSH1 CD4 T cells, which showed a reduced fold induction of these molecules after 18 h of activation (Fig. 7j, k and Supplementary Fig. 8b). Consistently, IL-2 production was also reduced in the cell culture supernatants of these cells (Fig. 7l). Taken together, these data support a role for SSH1 in regulating F-actin dynamics through Limk-1 activity in T cells (Fig. 8) and suggest a specific regulatory role for this phosphatase in facilitating TCR priming and T cell polarity, which in turn leads to full T cell activation.

Discussion

In this work, we provide experimental evidence for a regulatory role of SSH1 in cofilin activation during antigen-induced stimulation of T cells, and that this is mediated by downregulating Limk-1 activity. We show that SSH1 is recruited early at synaptic contacts established with B cells, where it localises to the peripheral area of the mature IS, as has been described for cofilin[12].

Late induced expression in the in vitro model used here indicates that this cytoskeleton regulator might contribute to cellular processes required for appropriate T cell immune responses such as cell division or metabolic reprogramming. These are interesting questions that deserve further research. Interestingly, an enhanced expression of SSH1 concomitant with a down-modulation of phosphorylated cofilin in Ser3 during differentiation of CD4 T cells is observed, and this is consistent with the role of SSH phosphatases in cofilin activation by dephosphorylation of this residue to fine-tune F-actin cytoskeleton rearrangements[34]. Once active, cofilin binds to actin filaments, severing them and facilitating their depolymerisation[35,36]. Cofilin has been shown to be activated by several receptors, including CD2 and CD28, providing a link between T cell surface receptors and cytoskeletal rearrangements[12]. However, direct intracellular regulators of cofilin during antigen-induced stimulation of T cells were not previously known. Cofilin is essential for the formation of local F-actin networks required for TCR activation and signalling[37]. In this context, our results show that Limk-1 deactivation by SSH1 is required for cofilin activation and F-actin rearrangements during human primary CD4 T cell activation. Resting E6-1 Jurkat CD4 T cells showed unaffected cofilin phosphorylation status following SSH1 depletion by CRISPR/Cas9 genome editing, in contrast to other cells where partial silencing of SSH1 by siRNA promoted an increment in phosphorylated cofilin[38]. A potential explanation is that cofilin dephosphorylation and activation depends on PI3K[34], which is hyperactivated due to defective expression of the phosphatase PTEN[39]. Limk-1 has been shown to promote cofilin inactivation by direct phosphorylation of Ser3, a process that allows F-actin stabilisation[36]. Remarkably, our data suggest that SSH1 could also control the stabilisation of the F-actin cytoskeleton through modulation of the Rac-PAK axis, which leads to Limk-1 activation. Thus, by activating cofilin and controlling PAK function, SSH1 promotes a fine-tuned local rearrangement of the actin cytoskeleton very early upon T-cell stimulation (model in Fig. 8).

SSH1 is inhibited by phosphorylation at residues S937 and S978 by protein kinase D (PKD) and interaction with 14-3-3 proteins, which blocks the interaction of the phosphatase with the actin cytoskeleton[36,40]. The PKC/PKD axis has been demonstrated in B and T lymphocytes[41]. In particular, PKD in T cells rapidly polarises to the centre of the IS driven by a gradient of DAG at this location[42]. Therefore, there may be a correlation between SSH1 localisation at peripheral sites of the mature synapse (here) and the re-localisation of PKD at the centre of the IS upon TCR/CD28 activation observed in other studies, which would be dependent on PI3K activity stimulated by CD28. Thus, the observed absence of SSH1 at the centre of the IS could be due to the removal of the protein from the centre of the IS upon phosphorylation by PKD. In Jurkat T cells, the absence of PTEN does not affect PKD activity[43,44] and then it is therefore plausible that this pathway controls the distribution of active SSH1 during the establishment of T cell synaptic contacts. Our data suggest that antigen-induced T cell stimulation triggers the rapid redistribution of SSH1 to regulate early T cell activation at the immunological synapse. The dynamics and determinants of SSH1 distribution within the different compartments of the immunological synapse should be further investigated. This distribution of SSH1 is dependent on F-actin dynamics integrity, while the accumulation of CD3ε remains in absence of actin polymerisation, consistent with previous observation[19]. Therefore, SSH1 at nascent cognate interactions allows proper cofilin activation, which would enable the formation and temporal regulation of local actin networks required for the proper recruitment and binding of Nck to CD3ε. Recent studies, which demonstrate the requirement of actin for Nck binding to CD3ε[7], support this proposed model. The Nck-CD3ε interaction occurs upon antigen engagement-induced αβ-TCR conformational change and stimulates actin reorganisation during T-cell spreading and immunological synapse assembly[6]. Binding of F-actin at cognate interactions would increase the catalytic activity of SSH1 against cofilin[45]. Therefore, cofilin would be efficiently activated to facilitate actin dynamics through the formation of new barbed ends and depolymerisation of pre-existing cortical actin structures. This would facilitate the establishment of the local actin network for the efficient recruitment of Nck. In this context, our data also suggest that F-actin integrity at the peripheral sites of the mature synapse is required for SSH1 polarisation.

The defective F-actin regulation, with increased speed of retrograde flow observed in *SSH1* KO cells also affects TCR/CD3, integrins and centrosome localisation at the IS. These data highlight the importance of rapid actin rearrangements not only for proper initial T cell contacts, but also for further reorganisation of the actin and tubulin cytoskeleton in mature IS. For the tubulin cytoskeleton, this may be achieved by requiring actin polymerisation to fix the centrosome at specific

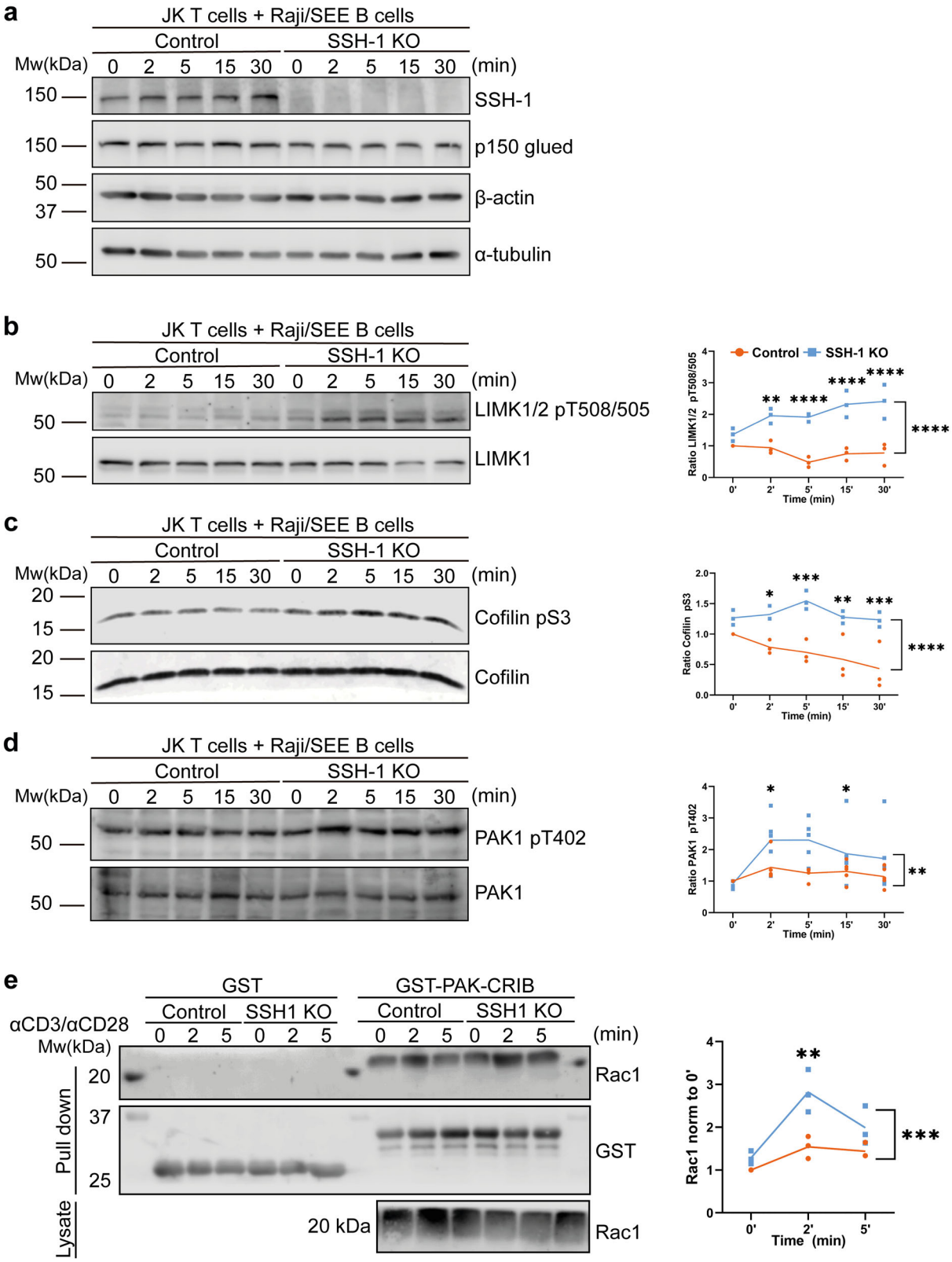

Fig. 5 | Limk-1 inactivation and cofilin activation downstream the TCR require SSH1. Western blot showing (**a**) SSH1 knockout, (**b**) phosphorylation of pT508/505 LIMK1/2 (**c**) pSer3 Cofilin and (**d**) pT402 PAK1 in control or *SSH1* KO JK T cells after conjugation with SEE-preloaded Raji cells for the indicated times. Graphs, ratio of phosphorylation to total protein normalised to unstimulated control. **e** Western blot of pull-down assay with GST-PAK-CRIB fusion protein as a bait for control or *SSH1* KO JK T cells. Activation was performed with soluble anti-CD3 and anti-CD28 antibodies for the indicated times. Rac1 and GST are shown. Rac1 levels in whole cell lysates are shown in the bottom row. Graph, quantification of Rac1 bands normalised to unstimulated control. Data are individual experiments shown as dots and lines representing the mean value; **a**–**c** $n = 3$; **d** $n = 5$; **e** $n = 3$, two-way ANOVA. $^{*}p < 0.05$; $^{**}p < 0.01$; $^{***}p < 0.001$; $^{****}p < 0.0001$.

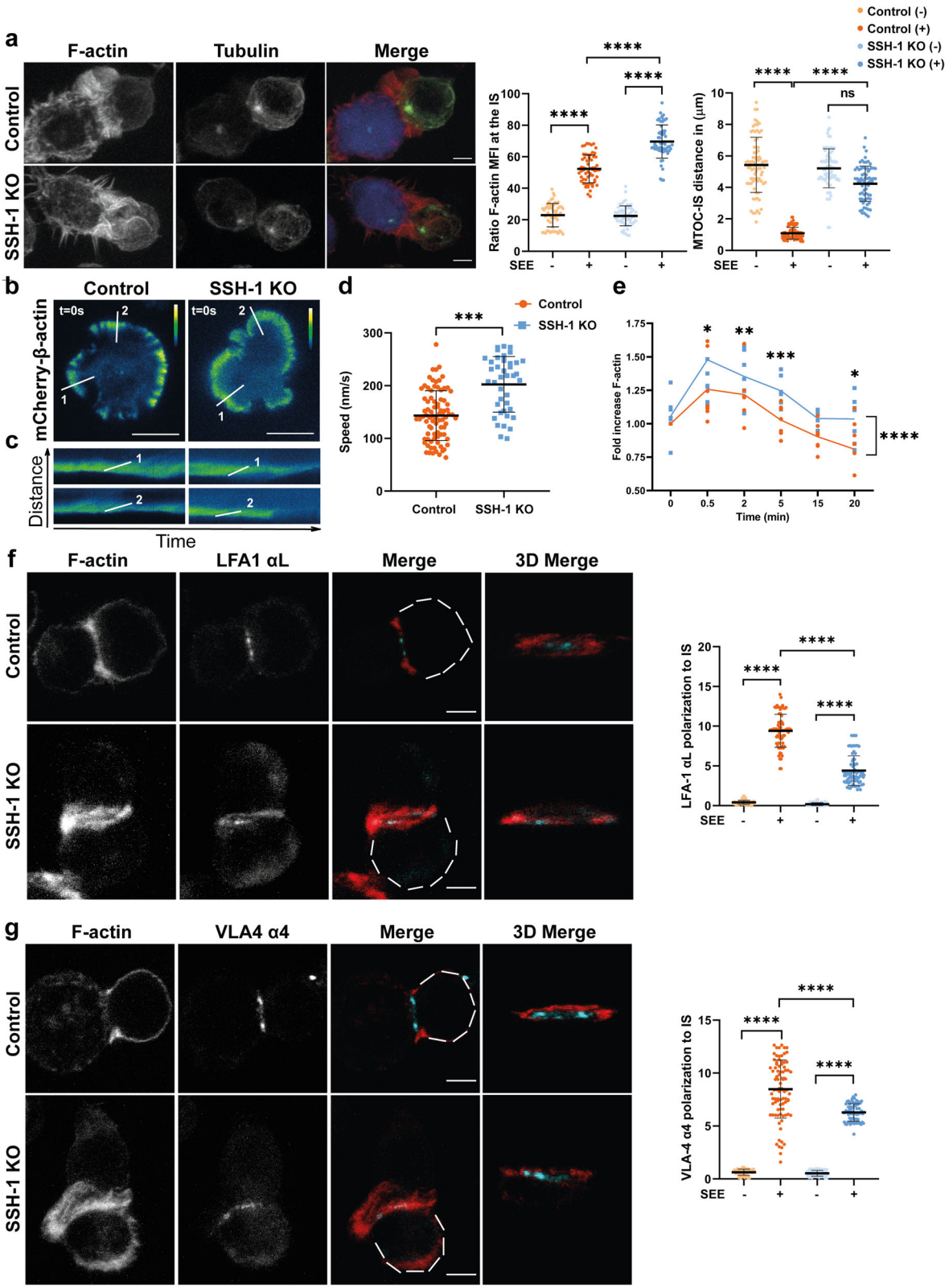

locations[46], which could be achieved by the ability of F-actin to organise a diffusion barrier around centrosomes[47], thus favouring the existence of different gradients of regulatory molecules at centrosomal and synaptic sites, as proposed[46,47]. An interesting model for achieving cell asymmetry at the IS is based on the ability of T cells to accumulate newly synthesised proteins at specific sites, such as centrosomes, early after TCR activation, without the need for gene expression[48]. In this context, the tubulin cytoskeleton is also regulated downstream of Limk-1[37,49], and the precise regulatory pathway for tubulin and actin by SSH1 and its impact on global asymmetric organisation should be investigated. Defective integrin positioning can also be explained by deregulated F-actin[50]. Indeed, it has recently been shown that the correct recruitment of LFA-1

Fig. 6 | SSH1 regulates F-actin dynamics and integrin localisation at the IS. **a** Fluorescence images of control and *SSH1* KO cells interacting with SEE-preloaded Raji cells. F-actin (red); α-tubulin (green); Raji cells (CMAC, blue). Bar, 5 μm. Graphs, ratios of F-actin MFI per contact area and MTOC distance to the APC. **b** Time-lapse TIRFm images from Video 2, showing control and *SSH1* KO cells expressing mCherry-β-actin (pseudocolour; time, 0 s). Bar, 10 μm. White lines indicate the location of numbered kymographs. **c** Kymographs of white lines in (**b**); Y, distance and X, time. **d** Graph, speed of retrograde flow at lamellipodia from (**b**, **c**). Symbols are single measurements. **e** Graph, F-actin polymerisation in control and *SSH1* KO cells activated with anti-CD3/anti-CD28 monoclonal antibodies expressed as fold increase of the averaged geometric mean normalised to unstimulated control. Confocal images of conjugates showing (**f**) LFA-1 αL integrin (cyan) and F-actin (red) and (**g**) VLA-4 α4 integrin (cyan) and F-actin (red). Bar, 5 μm. Graphs, accumulation of LFA-1 and VLA-4 at IS. Symbols are cell conjugates measured. Data, mean ± SD; **a** Ctrl(−) $n = 77$, Ctrl(+) $n = 85$, *SSH1* KO(−) $n = 77$, SSH1(+) $n = 75$, three independent experiments. Mann–Whitney test; **b**–**d** Ctrl $n = 84$; *SSH1* KO $n = 40$, three independent experiments, two-tailed unpaired *t*-test; **e** $n = 7$, two-way ANOVA; **f** Ctrl(−) $n = 82$, Ctrl(+) $n = 73$, *SSH1* KO(−) $n = 78$, *SSH1* KO(+) $n = 77$, three independent experiments. Mann–Whitney test; **g** Ctrl(−) $n = 75$, Ctrl(+) $n = 89$, *SSH1* KO(−) $n = 78$, *SSH1* KO(+) $n = 72$, three independent experiments. Mann–Whitney test; $^{*}p < 0.05$; $^{**}p < 0.01$; $^{***}p < 0.001$; $^{****}p < 0.0001$.

to the IS is dependent on cofilin[11]. However, based on the reduction in the actin flow mediated by the LFA-1/ICAM-1 interaction[28], the defective positioning of LFA-1 described here may also account for the observed increase in the speed of the actin retrograde flow.

Overall, findings presented here underscore SSH1 as a regulator of very early actin dynamics that drive T cell activation and proper organisation of the IS. Our data highlight a central role for SSH1 in fine-tuning early cytoskeletal rearrangements during T cell activation and co-stimulation. First, SSH1 activity on the Limk1-cofilin pathway directly promotes local actin rearrangements required for proper recruitment of Nck to allow further signalling downstream of the TCR (Fig. 8; left panel, green arrow). In this context, cofilin activation is also required for proper LFA-1 recruitment, which also contributes to early signalling. Secondly, SSH1 could control excessive activation of PAK (Fig. 8; left panel, red line), possibly originated from Nck[51,52], via PI3K downstream co-stimulation, where a potential positive feedback loop could occur via pCof/PLD[53]. The model presented here deserves further investigation, particularly with regard to the role of the SSH1 regulatory hub in the rearrangements of the tubulin cytoskeleton and the molecular reactions that lead to proper SSH1 activation downstream of the TCR and costimulatory interactions. In this context, it is important to note that the defective asymmetry observed in *SSH1* KO or SSH1 silenced cells has specific consequences on the activation of different signalling pathways, leading to a defective expression of genes indicating full T-cell activation, such as CD69, CD25 and IL-2 in primary CD4 T-cells.

Methods

Cells

The human Jurkat E6-1 CD4 T cell line (Vα1.2 Vβ8^{+} TCR) and CH7C17 CD4 T cell line (CH7; Jurkat-derived) (HAp-specific Vα1.4 Vβ3^{+} HA1.7 TCR)[54], and the lymphoblastoid B cell lines Raji (Burkitt lymphoma; obtained from the DSMZ Organisation; ACC-319) and HOM2 (Epstein-Barr virus transformed lymphoblastoid line; CVCL_A612) were cultured in RPMI 1640 + GlutaMAX–I + 25 mM HEPES (Gibco–Invitrogen) and supplemented with 10% fetal bovine serum (FBS) (Hyclone, Thermo Fisher). CH7C17 cells were grown in the presence of 4 μg/mL puromycin (Lonza) and 0.4 mg/mL hygromycin B (Lonza) to maintain expression of transfected HA-specific Vβ3 TCR. All lymphoid cell lines were routinely tested for specific expression of CD (clusters of differentiation) with specific antibodies by flow cytometry (Supplementary Fig. 4) and for mycoplasma infection by PCR.

Human peripheral blood mononuclear cells (PBMCs) were isolated from buffy coats of healthy donors by separation on a Biocoll gradient (Biochrom) according to standard procedures. Monocytes were separated from PBMCs by adherence for 30 min at 37 °C in RPMI supplemented with 10% FBS. Non-adherent cells were washed off and CD4 T cells were purified from PBMCs using an EasySep negative isolation kit for human CD4 T cells (Stem Cell Technologies). CD4 T cells were nucleofected with control or SSH1-specific siRNAs (2.5 μM) in Optimem[55] and used for activation assays 48 h post-transfection. T lymphoblasts were generated by either culturing CD4 T cells on RPMI 1640 containing 10% FBS, 100 U/mL penicillin, 100 μg/mL streptomycin and 2 mM L-glutamine (Lonza), in the presence of Dynabeads Human T-Activator CD3/CD28 (ratio 1:1) (Thermo Fisher Scientific) and 10 ng/mL IL-12 for 4 days, or by plating PBMCs at 1×10^{6} cells/mL in medium as before onto P24 wells in the presence of Staphylococcal Enterotoxin E (SEE), adding 50 U/mL IL-2 every 48 h, and allowing them to grow for 6 days. These studies were performed adhered to the principles of the Declaration of Helsinki and were approved by the local ethics committee for basic research at the '*Hospital La Princesa*' and '*Hospital Clinico de Madrid*'. Informed consent was obtained. All ethical regulations relevant to human research participants were followed.

Antibodies and reagents

The commercial primary antibodies used in this study were anti-phospho-CD3ζ Y83 (ab68236; 1:1000 for WB), anti-CD3ζ (ab190728; 1:1000 for WB), anti-phospho-LAT Y132 (ab4476; 1:1000 for WB) and anti-GFP (ab13970; 1:200 for IF) from Abcam; anti-β-actin (AM4302; clone AC-15; 1:2000 for WB), anti-α-tubulin (T6199; clone DM1A; 1:2000 for WB) and fluorescein isothiocyanate (FITC)-conjugated anti-α-tubulin (F2168; clone DM1A; 1:100 for IF) from Sigma-Aldrich; anti-ERK1/2 (SKU 13-6200; 1:500 for WB), anti-phospho-LIMK1/2 Y507/T508 (07-850; 1:500 for WB) and anti-PAK1 (71-9300; 1:500 for WB) were from Invitrogen; anti-phospho-ERK1/2 T202/Y204 (44285; 1:1000 for WB) was from Calbiochem; anti-Rac1 (610651; 1:500 for WB) and anti-p150^{glued} (610474; 1:500 for WB) were from BD Pharmingen; anti-phospho-PAK1 T402 (612-401-E05; 1:500 for WB) was from Rockland; anti-CD3ε (317302; clone OKT3; 1:200 for IF), anti-CD69-V450 (1:200 for FACS), anti-CD25-PE-Cy7 (1:200 for FACS), anti-CD19-APC (1:200 for FACS), anti-CD3-PE (1:200 for FACS) and anti-CD4-APC (1:200 for FACS) were from BioLegend; anti-cofilin (66057-1-Ig; 1:1000 for WB) was from Proteintech; anti-phospho-cofilin S3 (3311S; 1:1000 for WB), anti-phospho-ZAP70 Y493 (2704T; 1:1000 for WB), anti-ZAP70 (2705S; 1:1000 for WB), anti-phospho-SLP76 Y145 (14770; 1:1000 for WB), anti-PLCγ1 (2822S; 1:1000 for WB), anti-phospho-PLCγ1 Y783 (2821L;1:1000 for WB) and anti-SSH1 (13578S; 1:1000 for WB; 1:100 for IF) were from Cell Signaling Tech; anti-LIMK2 (sc-515585; 1:500 for WB) was from Santa Cruz Biotechnology. Ghost Dye™ Red 780 (13-0865; 1:500 for FACS) and Ghost Dye™ Violet 510 (13-0870; 1:500 for FACS) were from Tonbo Biosciences.

The following mAbs: anti-CD3ε (clone T3b), anti-CD3ε (clone APA1/1), which recognises the activation-dependent intracellular epitope of CD3ε, anti-CD11a (clone TP1/40) and anti-CD49d (clone HP2/1) were produced in our laboratory[56].

The anti-GST constructs, anti-GST antibody and the rabbit polyclonal Ab 448 (anti-human CD3ζ) were described previously[6]. Cell tracker CMAC (7-amino-4-chloromethylcoumarin; 10 μM, C2110) was from Molecular Probes, Invitrogen; SEE (0.5 μg/mL, PE404) was from Toxin Technologies; haemagglutinin peptide ($HAp_{210-219}$; 200 μg/mL) (sequence: TYVSVG TSTL) was synthesised by LifeTein, LLC; prolong gold antifade mounting medium (P-36934) and prolong gold antifade mounting medium with DAPI (P-36931) were from Thermo Fisher Scientific; Cytochalasin D (1 μM), latrunculin A (0.12 μM), fibronectin and poly-L-Lysine were from Sigma-Aldrich; recombinant ICAM-1 was from Hölzel Diagnostika Handels GmbH and human IL-2, IL-7 and IL-12 were purchased from PeproTech.

The following secondary reagents were used: phalloidin conjugated to Alexa Fluor 647 (A-22287; 1:40 for IF; 1:500 for FACS), phalloidin conjugated to Alexa Fluor 488 (A-12379; 1:40 for IF), goat anti-rabbit and goat anti-mouse highly cross-adsorbed secondary antibodies conjugated

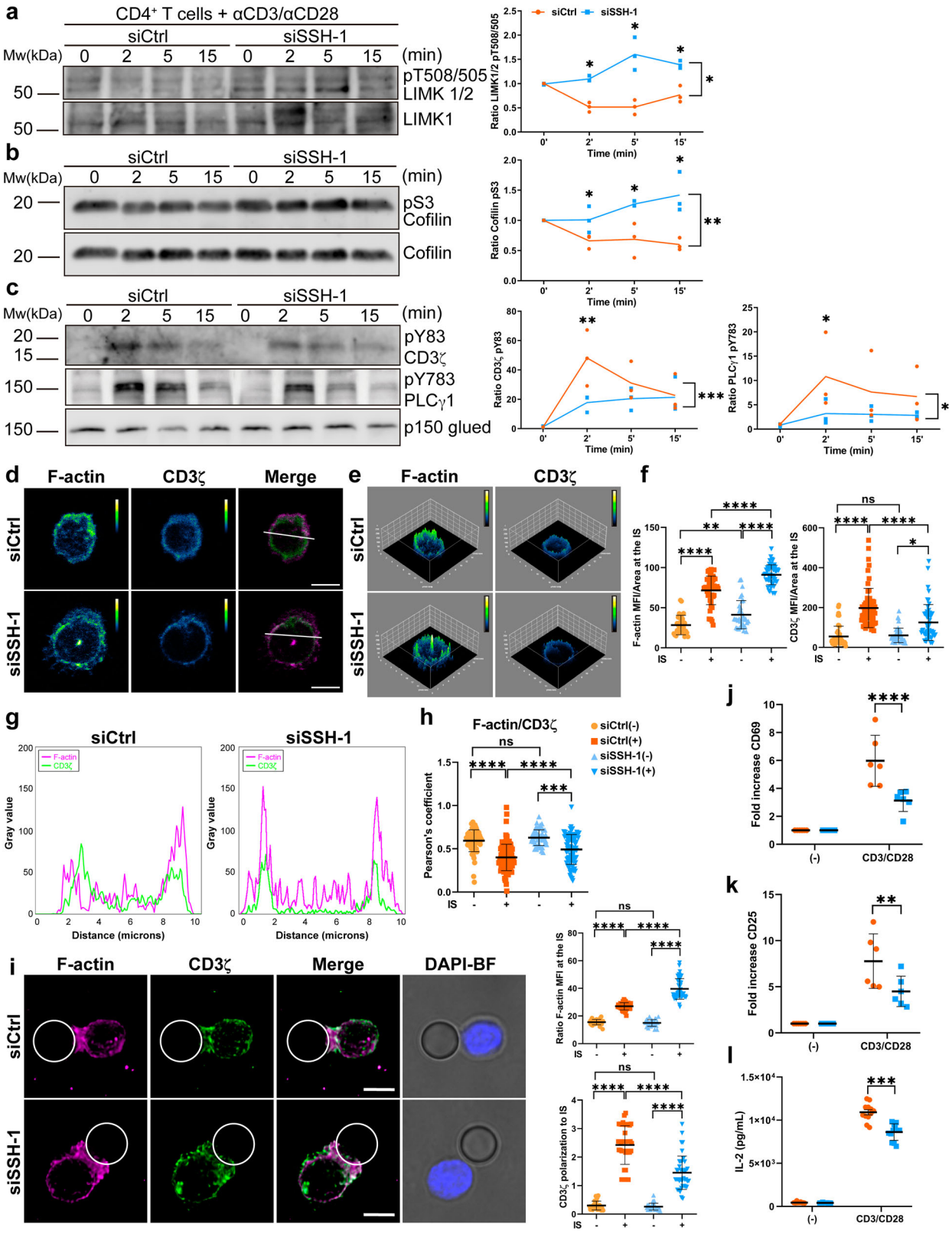

to Alexa Fluor 488 (A-11034 and A-11029, respectively; 1:500 for IF), 568 (A11036 and A-11031, respectively; 1:500 for IF) or 647 (A-21443 and A-21236, respectively; 1:500 for IF or FACS), donkey anti-goat highly cross-adsorbed secondary antibody conjugated to Alexa Fluor 647 (A-21447; 1:500 for IF), donkey anti-rabbit secondary antibody conjugated to Alexa Fluor 555 (A-31572; 1:500 for IF) and goat anti-chicken antibody conjugated to Alexa Fluor 488 (A-11039; 1:500 for IF) were purchased from Thermo Fisher Scientific; horseradish peroxidase(HRP)-conjugated secondary antibodies for WB (anti-rabbit 31460, anti-mouse 31430 or anti-goat IgG+IgM 31460; all 1:5000) were purchased from Thermo Fisher Scientific. Fluorescence-labelled secondary antibodies IRDye 680 goat anti-rabbit and IRDye 800 goat anti-mouse (926-68071 and 926-32350, respectively; 1:5000 for WB) were from LI-COR Bioscience.

Fig. 7 | SSH1 regulates cofilin and T-cell activation in CD4 T cells. Western blot showing the phosphorylation of (**a**) pT508/505 LIMK1/2, (**b**) pS3 cofilin, (**c**) pY83 CD3ζ and pY783 PLCγ1 in peripheral blood CD4 T cells obtained from individual donors, transfected with siCtrl and siSSH1 and stimulated with αCD3/αCD28 tetramers for the indicated times. Graphs, ratio of average phosphorylation to total protein normalised to unstimulated control. **d** Confocal fluorescence images of representative peripheral blood CD4 T cell transfected with siCtrl and siSSH1 and stimulated over surfaces coated with stimulatory anti-CD3/anti-CD28 monoclonal antibodies. F-actin (pseudocolour and magenta in the single and merged images, respectively) and CD3ζ (pseudocolour and green in the single and merged images, respectively) are shown. **e** 3D surface plots of (**d**) are shown. **f** Graphs, F-actin and CD3ζ MFI per area at the IS. Symbols are cells measured. **g** Graph, fluorescence intensity profile of F-actin and CD3ζ distribution at the IS shown in (**d**). **h** Graph, Pearson's correlation coefficient for co-localisation between F-actin and CD3ζ MFI at the IS. Symbols are cells measured. **i** Fluorescence images of CD4 T cells transfected with siCtrl and siSSH1 and conjugated with anti-CD3/anti-CD28-coated beads to establish IS. F-actin (magenta), CD3ζ (green), brightfield (BF) and DAPI (blue) are shown. Bar, 5 µm. Graphs, ratios of F-actin MFI and CD3ζ polarisation at the IS. **j–l** Peripheral blood CD4 T cells transfected with siCtrl and siSSH1 and stimulated or not with αCD3/αCD28 tetramers (18 h). Fold increase of the averaged geometric mean of (**j**) CD69 and (**k**) CD25 normalised to unstimulated control. **l** Concentration of IL-2 detected in supernatants. Data are individual experiments shown as dots and lines representing the mean value (**a–c**) or mean ± SD (**d–l**); **a–c** $n = 3$ independent donors, two-way ANOVA; **f** siCtrl $n = 59$, siSSH1 $n = 52$ cells analysed from four independent donors, Mann–Whitney test; **h** siCtrl $n = 111$, siSSH1 $n = 91$ cells analysed from four independent donors, two-tailed paired t-test; **i** siCtrl $n = 41$, siSSH1 $n = 44$ cells analysed from four independent donors, Mann–Whitney test; **j, k** $n = 6$; **l** $n = 12$ independent donors, two-tailed paired *t*-test. ns not significant, $^{*}p < 0.05$; $^{**}p < 0.01$; $^{****}p < 0.0001$. See also Supplementary Fig. 8.

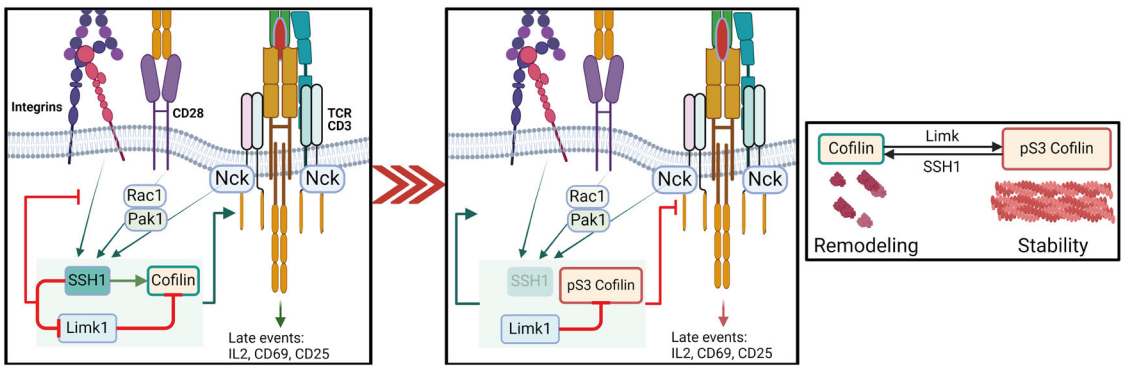

Fig. 8 | Model for the role of SSH1 during early T cell stimulation. Left panel: SSH1 inactivates Limk1 and modulates Rac1/PAK1 activation to further control Limk1 activity. This mechanism tunes cofilin action needed for proper Nck recruitment to the TCR. Right panel: SSH1 loss deregulates cofilin, resulting in decreased TCR signalling with F-actin stabilisation and hampered late events. Created with BioRender.com.

Generation of *SSH1* KO cells

CRISPR RNA (crRNA) were designed complementary to the early coding region of the *SSH1* gene using the online Benchling CRISPR gRNA design tool (http://www.benchling.com) (crRNA_1: CCACCACCATGTACCGGACCCGG & crRNA2: CACCGAGGAGAATATCTTGCTGG). The crRNA was complexed with the trans-activating RNA (tcrRNA) to form the guide RNA (gRNA). gRNA (3.3 µM) was incubated with Alt-R HiFi Cas9 Nuclease V3 (IDT) at 0.27 mg/mL and electroporated using the Neon Electroporation System (Thermo Fisher Scientific) as previously described[14]. Briefly, 2×10^5 Jurkat cells were electroporated using the following parameters: 1600 V, 10 ms, 3 pulses; after electroporation, the cells were maintained on antibiotic-free medium for 24 h and later cultured with fresh medium. Clones were obtained by limiting dilution, and SSH1 expression was measured by Western blot. Clones with no detectable levels of the protein were then mixed into an *SSH1* KO pool. To confirm the knockout, genomic DNA was amplified by PCR using a specific pair of primers *SSH1*_Fw: TCCAAAGGCAGGTTAGTGAGAG and *SSH1*_Rv: ACCTAGCCCATCAGACTCACC (Sigma-Aldrich). PCR products from control and *SSH1* KO samples were cloned and were sequenced to detect mutations in the edited region (Genomics facility of the Complutense University of Madrid, Spain).

Plasmids and siRNA transfections

The plasmid encoding the GFP-SSH1 fusion protein was previously described[14] and the plasmid encoding mCherry-CD3ζ was generated by Dr. Balbino Alarcon (Molecular Biology Centre Severo Ochoa, Spain). mCherry-β-actin (C-18) was a gift from Michael Davidson (Addgene plasmid, 54967). Double-stranded control (UUCUCCGAACGUGUGCACG and CGUGCACACGUUCGGAGAA) and SSH1-specific (CGGAGAACCUAAACAACAA and UUGUUGUUUAGGUUCUCCG) siRNAs were purchased from Eurogentec.

For Jurkat T cell transfection[57], cells were centrifuged at 1200 rpm for 5 min, washed with Hank's balanced salt solution (HBSS, Lonza) and resuspended in Opti- Mem I (Gibco–Invitrogen) (1×10^7 cells in 400 µL). Ten µg of plasmids or 2.5 µM siRNAs were added to the cell suspension, which was electroporated in a Gene-Pulse III system from Bio-Rad Laboratories set at 240 V, 975 mΩ. After electroporation, cells were resuspended in 5 mL RPMI 1640 + GlutaMAX–I + 25 mM HEPES medium + 5% FBS, plated in 25 cm^2 flasks and supplemented with 10% FBS after 3 h. Experiments were performed 24 h post-transfection.

Primary CD4 T cells (5×10^6 cells in 100 µL) were nucleofected with control or SSH1-specific siRNAs (2.5 µM) in pre-warmed Opti-MEM I (Gibco-Invitrogen) using the U-04 programme of Nucleofector I, (Amaxa) after a heat-shock step with cold HBSS (Hank's balanced salt solution). Cells were cultured for 48 h in RPMI 1640 supplemented with 10% FBS and IL-7 (10 ng/mL). Dead cells were discarded using Biocoll Separating Solution 24 h post-transfection. Experiments were performed 48 h post-transfection; specific silencing was verified by Western blot.

T cell activation and lysis for pull-downs and immunoblotting

For CD4 T cell or Jurkat activation, 1×10^6 cells per condition in 100 µL of RPMI were stimulated with 10 µL αCD3αCD28 tetramers (ImmunoCult™ Human CD3/CD28 T-Cell Activator; StemCell Technologies) for the indicated times. For the GST-Nck and GST-PAK-CRIB pull-down assays, 4×10^6 cells T cells in 200 µL of RPMI were stimulated with anti-CD3 (clone HIT3a, BioLegend) at 10 µg/mL plus anti-CD28 (clone CD28.2, BD Biosciences) at 3.33 µg/mL antibodies for the indicated times. Recombinant GST protein was then added to cell lysates in GST-Fish buffer (Tris-HCl 50 mM pH = 7.4 containing 100 mM NaCl, 1% NP-40, 2 mM $MgCl_2$, 10% glycerol and protease inhibitors) and pull-downs were performed as previously described[58]. For conjugate formation, 1×10^5 Raji cells were pulsed with 0.5 µg/mL SEE (1 h, 37 °C, complete medium), washed and mixed with

1×10^6 E6-1 Jurkat T cells (1:10) or 1×10^5 HOM2 were loaded with 200 µg/mL HAp (2 h, 37 °C, complete medium) and then conjugated with siCtrl or siSSH1 CH7C17 Jurkat T cells (1:10) for the indicated times. Cells were centrifuged at 800 rpm at 37 °C to promote conjugate formation. A total of 1×10^6 cells were lysed in 50 µL of 5 mM Tris-HCl pH 7.5 containing 1% NP40, 0.2% Triton X-100, 150 mM NaCl, 2 mM EDTA, 1.5 mM $MgCl_2$, and phosphatase and protease inhibitors (Sigma-Aldrich) for 30 min on ice followed by a preclearance step by centrifugation at 14,000 rpm (4 °C, 10 min) to remove debris and nuclei. Samples were processed for SDS-PAGE, transferred to nitrocellulose membranes, and incubated with appropriate primary (o/n, 4 °C) and peroxidase-labelled secondary antibodies (1 h, RT). Chemiluminescence was detected using the Amersham 880 detection system (GE Healthcare). For fluorescent Western blot, IRDye 680 goat anti-rabbit and IRDye 800 goat anti-mouse secondary antibodies (Li-Cor Biosciences) were also incubated for 1 h at RT and detected using the Odyssey® Infrared Imager (LI-COR Bioscience).

For the analysis of protein expression after T cell differentiation and the verification of CRISPR in E6-1 Jurkat cells, cells were lysed in ice-cold 20 mM Tris-HCl pH 7.5 buffer, containing 1% NP40, 0.1% SDS, 0.5% sodium deoxycholate (SDS) and phosphatase and protease inhibitors (Phosphostop and Complete tablets from Roche, respectively) for 30 min on ice followed by a sonication step (Sonics & Materials Inc; 3 pulses of 10 s at 20% amplitude). Proteins were resolved by SDS–PAGE and transferred to PVDF membranes. After blocking with TBS containing 0.2% Tween and 5% BSA, the membranes were blotted with primary antibodies (o/n, 4 °C) followed by either peroxidase-labelled or fluorescence-labelled secondary antibodies (1 h, RT). Chemiluminescence or fluorescence was detected using the Odyssey® Infrared Imager (LI-COR Bioscience).

Densitometric analysis and quantification of Western blots

Bands from Western blots were quantified (arbitrary units per pixel) using either the supplied Image Gauge (Fujifilm Inc) or Image Studio Lite (v5.2, LI-COR Biosciences) softwares. Background was subtracted and the resulting values were normalised to unstimulated control samples. The data obtained were statistically analysed and plotted using PRISM8 (GraphPad software).

Cell conjugate formation and immunofluorescence experiments

For cell conjugate formation[57,59], Raji B cells were washed once with HBSS and loaded with the CMAC cell tracker (10 µM; Molecular Probes) and with SEE (0.5 µg/mL; Toxin Technologies) for 1 h at 37 °C. The cell conjugates were then attached to poly-L-Lys-coated coverslips for 30 min at 37 °C. CD4 T cells were incubated for 30 min at 37 °C on coverslips coated with αCD3 (clone HIT3a, BioLegend) at 10 µg/mL and αCD28 (clone CD28.2, BD Biosciences) at 3.33 µg/mL or conjugated with anti-CD3ε mAb (10 µg/mL; HIT3a clone) and anti-CD28 mAb (3.33 µg/mL; CD28.2 clone) coated latex microbeads (6.4 µm in diameter, Sigma-Aldrich) for 30 min at 37 °C and were allowed to spread over poly-L-Lys-coated coverslips. Controls were CD4 T cells conjugated with human γ-globulin (100 µg/mL) coated beads. Cells were then fixed with 4% paraformaldehyde in PHEM (PIPES 30 mM, HEPES 20 mM, EGTA 2 mM, $MgCl_2$ 1 mM, pH: 6.9) containing 0.12 M sucrose for 10 min (R/T), permeabilised with TX-100 (0.2%) in PHEM for 5 min at R/T and blocked with PHEM containing 100 µg/mL γ-globulin, 3% BSA, 0.2% azide for 30 min at R/T. Cells were sequentially stained with the indicated primary antibodies (1–10 µg/mL) followed by Alexa Fluor 488-, 568- or 647-conjugated secondary antibodies (4 µg/mL), Alexa-conjugated phalloidin (5 µg/mL) or fluorescein isothiocyanate (FITC)-conjugated anti-α-tubulin (0.1 µg/mL). Samples were mounted on Prolong gold or Prolong gold-DAPI (Invitrogen). A series of fluorescence and brightfield images were captured using a TCS SP5 confocal laser scanning unit (Leica Microsystems) attached to an inverted epifluorescence microscope (DMI6000) fitted with an HCX PL APO 63x/1.40-0.6 oil objective. Epifluorescence images from CD4 T cells conjugated with latex microbeads were acquired as a Z-series of fluorescence and brightfield images under a THUNDER Imager Live Cell & 3D Cell Culture & 3D Assay and processed with the accompanying thunder algorithm for deconvolution (Leica Microsystems). A 100x objective was used.

To disrupt the actin cytoskeleton, conjugates were incubated for 5 min before the addition of 0.12 µM latrunculin A (Lat-A) or 1 µM cytochalasin D (Cyto-D), and then incubated for a further 10 min before fixation. For live imaging, CH7C17 cells were co-transfected with plasmids encoding GFP-SSH1 and mCherry-CD3ζ. Transfected cells were added into poly-L-lysine-coated chambers. CMAC-stained HOM2 cells were loaded with HAp for 2 h at 37 °C and added to the chambers under the microscope and time-lapse confocal microscopy was performed with a FV1100 confocal microscope (Olympus). Confocal sections were acquired with elapsed times of 10 s. The different fluorophores were excited at 405 nm (CMAC), 488 nm (GFP), 594 nm (mCherry) and 647 nm (Phalloidin-647).

Images were processed using Image J software (http://rsbweb.nih.gov/ij/). The *'Synapse Measures'* plugin (http://rsbweb.nih.gov/ij/) was used to quantify protein accumulation at the contact area[60]. This programme provides accurate measurements of localised immunofluorescence by comparing fluorescence signals from multiple regions of the T cell, APC, IS and after subtraction of background fluorescence. Maximal projections and 3D analysis of the T cell-APC contact area were generated using *'Z-project', 'Reslice' and '3D surface plot'* functions of Image J. Colocalisation was measured by using the built-in tool *'Colocalization threshold'*. The distance of the centrosome to the IS was calculated using IMARIS 8.4 software (https://imaris.oxinst.com) by calculating volumes based on MFI and using the matlab implemented utility 'spots to volume distance'[61].

TIRFm and image analysis

For total internal reflection fluorescence microscopy (TIRFm), control and *SSH1* KO cells were transfected with Neon technology to overexpress mCherry-β-actin. Cells were incubated for 24 h, washed, and cultured in Hank's balanced salt solution supplemented with FBS (1%) and HEPES (25 mM). Cells were then seeded onto glass-bottom dishes coated with stimulatory anti-CD3ε monoclonal antibody (clone UCHT-1) and recombinant ICAM-1. Imaging was performed using a Leica AM TIRF MC M 329 system (Leica Microsystems) mounted on a Leica DMI 6000B microscope coupled to an Andor-DU8285 VP-4094 camera, fitted with an HCX PL APO 100.0×1.46 immerse oil objective and a Z penetrance of 150 nm. mCherry in the samples was excited with the 560 nm laser. The elapsed time of videos was 90 ms. To estimate the speed of actin in TIRFm images, kymographs were created from the radius of the cell, and a line was drawn, following the signal of interest signal, to measure its angle and length[59]. The speed of actin was calculated using the following trigonometric function, where the hypotenuse (H) is the length of the drawn line, the catheti are the distance (Catd) and time (Catt), and the measured angle is the angle between the hypotenuse and Catd (θ):

$$\text{Catd} = \text{Cosine}(\theta) \times H$$

$$\text{Catt} = \text{Sine}(\theta) \times H$$

Flow cytometry staining

A total of $1–2 \times 10^5$ cells of each cellular type were employed in each flow cytometry staining. Primary and secondary antibody staining was maintained for 30 min on ice and washed with FACS buffer (HBSS, 50 µg/mL human γ-globulin, 2% BSA, 1 mM EDTA). For intracellular F-actin and APA1/1 detection by flow cytometry, 5×10^5 cells were activated in high binding flat bottom, 96-well plates coated with αCD3 (clone HIT3a, BioLegend) at 10 µg/mL and αCD28 (clone CD28.2, BD Biosciences) at 3.33 µg/mL for corresponding times, and then fixed with fixation buffer (BioLegend) for

30 min on ice. Cells were then washed with permeabilisation buffer (BioLegend) and incubated with Alexa 647-conjugated phalloidin or APA 1/1 antibody followed by Alexa Fluor 647-labelled secondary antibody for 30 min on ice in permeabilisation buffer. For CD69 and CD25 surface expression detection by flow cytometry in primary CD4 T cells or in conjugates of Jurkat and Raji cells, CD4 T cells were activated with αCD3αCD28 Immunocult for 18 h or 1×10^5 Raji cells were loaded with 0.5 µg/mL SEE for 1 h and then conjugated with Jurkat cells at 1:1 ratio in U-bottom 96-well plate for 18 h at 37 °C and 5% CO_2. Cells were then washed with FACS buffer and stained with fluorophore-labelled primary antibodies for 30 min on ice. Finally, cells were resuspended in 200 µL of FACS buffer for flow cytometry acquisition. Data were acquired using a FACSCanto II analyser cytometer (405 nm violet laser, 488 nm solid state blue laser and 633 nm He-Ne) (BD Biosciences) and analysed using FlowJo software v10.8.1 (BD Biosciences).

ELISA

Supernatants of Jurkat cells conjugated with Raji for 18 h[59] or primary CD4 T cells activated with αCD3αCD28 Immunocult for 18 h were collected and diluted 1:5 or 1:10 respectively and stored at −80 °C until analysis. IL-2 detection was performed by ELISA (Human IL-2 ELISA Kit, Diaclone, 851500010) according to manufacturer's instructions. The results were quantified in an ELx800 absorbance microplate reader (Promega). Absorbance values were interpolated in a standard curve using Excel software.

Statistics and reproducibility

Statistical analyses were performed using PRISM8 (GraphPad software). Normality tests were performed to apply Student's *t* test or Mann–Whitney test when comparing two samples. When comparing two or more samples, including time courses, two-way ANOVA was used. Specific details of each analysis are given in the figure legends. Significant differences were considered when $p < 0.05$ (*); ** indicates $p < 0.01$; ***$p < 0.001$ and ****$p < 0.0001$.

Reporting summary

Further information on research design is available in the Nature Portfolio Reporting Summary linked to this article.

Data availability

The data underlying this article are available in the article and in its Supplementary Information. Numerical data source is provided in the Supplementary data. All other data and source data are available from the corresponding authors on reasonable request.

Received: 12 February 2024; Accepted: 19 July 2024;
Published online: 30 July 2024

References

1. Cai, E. et al. Visualizing dynamic microvillar search and stabilization during ligand detection by T cells. *Science* **356**, eaal3118 (2017).
2. Martín-Cófreces, N. B., Alarcón, B. & Sánchez-Madrid, F. Tubulin and actin interplay at the T cell and antigen-presenting cell interface. *Front. Immunol.* **2**, 24 (2011).
3. Huang, Y. & Burkhardt, J. K. T-cell-receptor-dependent actin regulatory mechanisms. *J. Cell Sci.* **120**, 723–730 (2007).
4. Comrie, W. A. & Burkhardt, J. K. Action and traction: cytoskeletal control of receptor triggering at the immunological synapse. *Front. Immunol.* **7**, 68 (2016).
5. Kumari, S. et al. Actin foci facilitate activation of the phospholipase C-γ in primary T lymphocytes via the WASP pathway. *Elife* **4**, e04953 (2015).
6. Gil, D., Schamel, W. W., Montoya, M., Sánchez-Madrid, F. & Alarcón, B. Recruitment of Nck by CD3 epsilon reveals a ligand-induced conformational change essential for T cell receptor signaling and synapse formation. *Cell* **109**, 901–912 (2002).
7. Wipa, P. et al. Actin polymerization regulates recruitment of Nck to CD3ε upon T-cell receptor triggering. *Immunology* **159**, 298–308 (2020).
8. Ghosh, M. et al. Cofilin promotes actin polymerization and defines the direction of cell motility. *Science* **304**, 743–746 (2004).
9. Lee, K. H., Meuer, S. C. & Samstag, Y. Cofilin: a missing link between T cell co-stimulation and rearrangement of the actin cytoskeleton. *Eur. J. Immunol.* **30**, 892–899 (2000).
10. Kim, J. et al. Coactosin-like 1 antagonizes cofilin to promote lamellipodial protrusion at the immune synapse. *PLoS ONE* **9**, e85090 (2014).
11. Wabnitz, G. H. et al. LFA-1 cluster formation in T-cells depends on L-plastin phosphorylation regulated by P90RSK and PP2A. *Cell. Mol. Life Sci.* **78**, 3543–3564 (2021).
12. Eibert, S. M. et al. Cofilin peptide homologs interfere with immunological synapse formation and T cell activation. *Proc. Natl Acad. Sci. USA* **101**, 1957–1962 (2004).
13. Wabnitz, G. H. et al. Protein phosphatase 1α and cofilin regulate nuclear translocation of NF-κB and promote expression of the anti-inflammatory cytokine interleukin-10 by T cells. *Mol. Cell Biol.* **38**, e00041–18 (2018).
14. Ramirez-Munoz, R., Castro-Sánchez, P. & Roda-Navarro, P. Ultrasensitivity in the cofilin signaling module: a mechanism for tuning T cell responses. *Front. Immunol.* **7**, 59 (2016).
15. Seeland, I. et al. The actin remodeling protein cofilin is crucial for thymic αβ but not γδ T-cell development. *PLoS Biol.* **16**, e2005380 (2018).
16. Samstag, Y. & Nebl, G. Interaction of cofilin with the serine phosphatases PP1 and PP2A in normal and neoplastic human T lymphocytes. *Adv. Enzym. Regul.* **43**, 197–211 (2003).
17. Mizuno, K. Signaling mechanisms and functional roles of cofilin phosphorylation and dephosphorylation. *Cell Signal.* **25**, 457–469 (2013).
18. Shoji, K., Ohashi, K., Sampei, K., Oikawa, M. & Mizuno, K. Cytochalasin D acts as an inhibitor of the actin-cofilin interaction. *Biochem. Biophys. Res. Commun.* **424**, 52–57 (2012).
19. Varma, R., Campi, G., Yokosuka, T., Saito, T. & Dustin, M. L. T cell receptor-proximal signals are sustained in peripheral microclusters and terminated in the central supramolecular activation cluster. *Immunity* **25**, 117–127 (2006).
20. Smith-Garvin, J. E., Koretzky, G. A. & Jordan, M. S. T cell activation. *Annu. Rev. Immunol.* **27**, 591–619 (2009).
21. Malissen, B., Grégoire, C., Malissen, M. & Roncagalli, R. Integrative biology of T cell activation. *Nat. Immunol.* **15**, 790–797 (2014).
22. Beach, D., Gonen, R., Bogin, Y., Reischl, I. G. & Yablonski, D. Dual role of SLP-76 in mediating T cell receptor-induced activation of phospholipase C-gamma1. *J. Biol. Chem.* **282**, 2937–2946 (2007).
23. Koyasu, S. et al. Phosphorylation of multiple CD3 zeta tyrosine residues leads to formation of pp21 in vitro and in vivo. Structural changes upon T cell receptor stimulation. *J. Biol. Chem.* **267**, 3375–3381 (1992).
24. DeFord-Watts, L. M. et al. The CD3 zeta subunit contains a phosphoinositide-binding motif that is required for the stable accumulation of TCR-CD3 complex at the immunological synapse. *J. Immunol.* **186**, 6839–6847 (2011).
25. Olazabal, I. M. et al. Activation outcomes induced in naïve CD8 T-cells by macrophages primed via "phagocytic" and nonphagocytic pathways. *Mol. Biol. Cell* **19**, 701–710 (2008).
26. Edwards, D. C., Sanders, L. C., Bokoch, G. M. & Gill, G. N. Activation of LIM-kinase by Pak1 couples Rac/Cdc42 GTPase signalling to actin cytoskeletal dynamics. *Nat. Cell Biol.* **1**, 253–259 (1999).
27. Sander, E. E., ten Klooster, J. P., van Delft, S., van der Kammen, R. A. & Collard, J. G. Rac downregulates Rho activity: reciprocal balance between both GTPases determines cellular morphology and migratory behavior. *J. Cell Biol.* **147**, 1009–1022 (1999).

28. Jankowska, K. I. et al. Integrins modulate T cell receptor signaling by constraining actin flow at the immunological synapse. *Front. Immunol.* **9**, 25 (2018).
29. Dustin, M. L. & Cooper, J. A. The immunological synapse and the actin cytoskeleton: molecular hardware for T cell signaling. *Nat. Immunol.* **1**, 23–29 (2000).
30. Tabdanov, E. et al. Micropatterning of TCR and LFA-1 ligands reveals complementary effects on cytoskeleton mechanics in T cells. *Integr. Biol.* **7**, 1272–1284 (2015).
31. Calderwood, D. A., Shattil, S. J. & Ginsberg, M. H. Integrins and actin filaments: reciprocal regulation of cell adhesion and signaling. *J. Biol. Chem.* **275**, 22607–22610 (2000).
32. Nordenfelt, P., Elliott, H. L. & Springer, T. A. Coordinated integrin activation by actin-dependent force during T-cell migration. *Nat. Commun.* **7**, 13119 (2016).
33. Murugesan, S. et al. Formin-generated actomyosin arcs propel T cell receptor microcluster movement at the immune synapse. *J. Cell Biol.* **215**, 383–399 (2016).
34. Eiseler, T. et al. Protein kinase D1 regulates cofilin-mediated F-actin reorganization and cell motility through slingshot. *Nat. Cell Biol.* **11**, 545–556 (2009).
35. Niwa, R. et al. Control of actin reorganization by Slingshot, a family of phosphatases that dephosphorylate ADF/cofilin. *Cell* **108**, 233–246 (2002).
36. Nagata-Ohashi, K. et al. A pathway of neuregulin-induced activation of cofilin-phosphatase Slingshot and cofilin in lamellipodia. *J. Cell Biol.* **165**, 465–471 (2004).
37. Gorovoy, M. et al. LIM kinase 1 coordinates microtubule stability and actin polymerization in human endothelial cells. *J. Biol. Chem.* **280**, 26533–26542 (2005).
38. Nishita, M. et al. Spatial and temporal regulation of cofilin activity by LIM kinase and Slingshot is critical for directional cell migration. *J. Cell Biol.* **171**, 349–359 (2005).
39. Blumenthal, D. & Burkhardt, J. K. Multiple actin networks coordinate mechanotransduction at the immunological synapse. *J. Cell Biol.* **219**, e201911058 (2020).
40. Peterburs, P. et al. Protein kinase D regulates cell migration by direct phosphorylation of the cofilin phosphatase slingshot 1 like. *Cancer Res.* **69**, 5634–5638 (2009).
41. Rozengurt, E., Rey, O. & Waldron, R. T. Protein kinase D signaling. *J. Biol. Chem.* **280**, 13205–13208 (2005).
42. Spitaler, M., Emslie, E., Wood, C. D. & Cantrell, D. Diacylglycerol and protein kinase D localization during T lymphocyte activation. *Immunity* **24**, 535–546 (2006).
43. Shan, X. et al. Deficiency of PTEN in Jurkat T cells causes constitutive localization of Itk to the plasma membrane and hyperresponsiveness to CD3 stimulation. *Mol. Cell Biol.* **20**, 6945–6957 (2000).
44. Freeley, M. et al. Loss of PTEN expression does not contribute to PDK-1 activity and PKC activation-loop phosphorylation in Jurkat leukaemic T cells. *Cell Signal.* **19**, 2444–2457 (2007).
45. Takahashi, K., Kanno, S. & Mizuno, K. Activation of cytosolic Slingshot-1 phosphatase by gelsolin-generated soluble actin filaments. *Biochem. Biophys. Res. Commun.* **454**, 471–477 (2014).
46. Yamamoto, S. et al. Actin network architecture can ensure robust centering or sensitive decentering of the centrosome. *EMBO J.* **41**, e111631 (2022).
47. Cheng, H. et al. Actin filaments form a size-dependent diffusion barrier around centrosomes. *EMBO Rep.* **24**, e54935 (2023).
48. Martin-Cofreces, N. B., Valpuesta, J. M. & Sánchez-Madrid, F. T cell asymmetry and metabolic crosstalk can fine-tune immunological synapses. *Trends Immunol.* **42**, 649–653 (2021).
49. Ray, S., Fanti, J. A., Macedo, D. P. & Larsen, M. LIM kinase regulation of cytoskeletal dynamics is required for salivary gland branching morphogenesis. *Mol. Biol. Cell* **25**, 2393–2407 (2014).
50. Comrie, W. A., Babich, A. & Burkhardt, J. K. F-actin flow drives affinity maturation and spatial organization of LFA-1 at the immunological synapse. *J. Cell Biol.* **208**, 475–491 (2015).
51. Yablonski, D., Kane, L. P., Qian, D. & Weiss, A. A Nck-Pak1 signaling module is required for T-cell receptor-mediated activation of NFAT, but not of JNK. *EMBO J.* **17**, 5647–5657 (1998).
52. Lin, J. & Weiss, A. T cell receptor signalling. *J. Cell Sci.* **114**, 243–244 (2001).
53. Han, L. et al. Direct stimulation of receptor-controlled phospholipase D1 by phospho-cofilin. *EMBO J.* **26**, 4189–4202 (2007).
54. Hewitt, C. R. et al. Major histocompatibility complex independent clonal T cell anergy by direct interaction of Staphylococcus aureus enterotoxin B with the T cell antigen receptor. *J. Exp. Med.* **175**, 1493–1499 (1992).
55. Martín-Cófreces, N. B., Rojas-Gomez, A., Dosil, S. G., Fernandez-Delgado, I. & Sánchez-Madrid, F. Rapid visualization of intracellular vesicle events during synaptic stimulation. *Methods Mol. Biol.* **2346**, 105–120 (2021).
56. Mittelbrunn, M. et al. VLA-4 integrin concentrates at the peripheral supramolecular activation complex of the immune synapse and drives T helper 1 responses. *Proc. Natl Acad. Sci. USA* **101**, 11058–11063 (2004).
57. Gómez-Morón, A., Requena, S., Roda-Navarro, P. & Martín-Cófreces, N. B. Activation kinetics of regulatory molecules during immunological synapse in T cells. *Methods Cell Biol.* **178**, 149–171 (2023).
58. Vicente-Manzanares, M. et al. Control of lymphocyte shape and the chemotactic response by the GTP exchange factor Vav. *Blood* **105**, 3026–3034 (2005).
59. Carrasco-Padilla, C. et al. T cell activation and effector function in the human Jurkat T cell model. *Methods Cell Biol.* **178**, 25–41 (2023).
60. Calabia-Linares, C. et al. Endosomal clathrin drives actin accumulation at the immunological synapse. *J. Cell Sci.* **124**, 820–830 (2011).
61. Blas-Rus, N., Bustos-Morán, E., Sánchez-Madrid, F. & Martín-Cófreces, N. B. Analysis of microtubules and microtubule-organizing center at the immune synapse. *Methods Mol. Biol.* **1584**, 31–49 (2017).

Acknowledgements

This study was supported by grants from Madrid Regional Government (Y2018/BIO-5207_SINERGY_CAM) to P.R.N. and (S2022/BMD-7209-INTEGRAMUNE-CM) to N.B.M.C., from Spanish Ministry of Science and Innovation in part granted with ERDF 'A way of making Europe' (SAF2016-75656-P and PID2020-115444GB-I00) to P.R.N. and (MCIN/AEI/10.13039/501100011033) PID2022–141895OB-I00 to N.B.M.C. N.B.M.C. and F.S.M. are also funded by Fundación La Caixa (LCF/PR/HR23/52430018) and CIBER Cardiovascular (Fondo de Investigación Sanitaria del Instituto de Salud Carlos III and co-funded by Fondo Europeo de Desarrollo Regional FEDER). A.G.M. is supported by an Investigo Grant (2022-C23.I01.P03.S0020000003) by SEPE (Fondos de Resiliencia), Gobierno de España to N.B.M.C. S.A.G., O.A.S. and C.C.P. are supported by a Ph.D. Fellowship from UCM. R.R.M. is supported by SAF2012-33218 to P.R.N. C.S. is supported by PEJ-2021-TL/BMD-21204 'Garantía Juvenil' grant to N.B.M.C. from Comunidad de Madrid. A.H.E. is supported by 'Contrato Investigo' from the 'Comunidad de Madrid' (CT36/22-79-UCM-INV) to P.R.N. The Centro Nacional de Investigaciones Cardiovasculares (CNIC) is supported by the ISCIII, the Ministerio de Ciencia e Innovación and the Pro CNIC Foundation. The CNIC is a Severo Ochoa Center of Excellence (MINECO award CEX2020-001041-S). Work in the SRP laboratory is funded by Asociación Española Contra el Cancer (LABAE20049RODR to S.R.P.); Spanish National Research and Development Plan, Instituto de Salud Carlos III and FEDER (PI20/01837 to S.R.P. and PI21/01641 to R.T.R.). Funding agencies have not intervened in the design of the studies, with no copyright over the study. Optical microscopy experimentation was conducted at the (1) Unidad de Citometría de Flujo y Microscopía de Fluorescencia, CAI-

UCM, (2) the Microscopy & Dynamic Imaging, CNIC, ICTS-ReDib, cofunded by MCIN/AEI/10.13039/501100011033 and FEDER 'Una manera de hacer Europa' (#ICTS-2018-04-CNIC-16) and (3) the Videomicroscopy Facility of the IIS-IP (Madrid, Spain), co-funded by IFEQ21/00085 and IFCS22/00014 from ISCIII and FEDER. We are grateful to Ms. M Ángeles Vallejo for her helpful assistance and management and Dr. JL Rodriguez-Fernandez (CIB-CSIC) for technical advice and critical reading of the manuscript.

Author contributions

A.G.M.: experimental design and execution, data curation (cell biology, transfection/nucleofection, flow cytometry, pull-down assays, Western blot and confocal microscopy), image composition, writing (original draft, review and editing), Figs. 3–8 and Supplementary Figs. 2, 4–8; S.A.G.: experimental design and execution, data curation (CRISPR/Cas9-based editing, cell biology and Neon transfection, microscopy, Western blot, flow cytometry), image composition, writing (original draft, review and editing), Figs. 1 and 2, Supplementary Figs. 1 and 3 and Supplementary Movie 1; R.R.M. performed experiments and data curation (TIRFm), Figs. 2a, b, 6b–d and Supplementary Movie 2; C.S. performed experiments, (Pull-down assay, and Thunder microscopy), Figs. 4, 5, 7 and Supplementary Figs. 4, 6; A.H.E., M.G.G., O.A.S. and C.C.P. performed experiments (flow cytometry, microscopy), Fig. 6; A.B. contributed valuable reagents and wrote revised draft; R.T.R. and S.R.P. performed CRISPR/Cas9-based editing, Supplementary Fig. 3; F.S.M.: resources, funding acquisition, data curation, revised manuscript; P.R.N. and N.B.M.C. planned and coordinated research, conceptualisation, resources, funding acquisition, data curation, analysed and interpreted data and wrote the manuscript with input from all authors. All authors contributed to the article and approved the submitted version.

Competing interests

The authors declare no competing interests.

Ethical approval

These studies were performed according to the principles of the Declaration of Helsinki and approved by the local Ethics Committee for Basic Research at the *Hospital La Princesa* (Madrid) and *Hospital Clinico* (Madrid).

Consent to publish

Consent to publish has been received from all participants.

Additional information

Supplementary information The online version contains supplementary material available at https://doi.org/10.1038/s42003-024-06605-8.

Correspondence and requests for materials should be addressed to Noa Beatriz Martín-Cófreces or Pedro Roda-Navarro.

Peer review information *Communications Biology* thanks Zeyang Liu and the other, anonymous, reviewer(s) for their contribution to the peer review of this work. Primary Handling Editors: X Frank Zhang and Dario Ummarino. A peer review file is available.